EUROPEAN ORGANIZATION FOR NUCLEAR RESEARCH

CERN-EP/82-16
12 February 1982

MUON DIFFUSION AND TRAPPING IN ALUMINIUM AND DILUTE ALUMINIUM ALLOYS: EXPERIMENTS AND COMPARISON WITH SMALL-POLARON THEORY

K.W. Kehr, D. Richter and J.-M. Welter
Institut für Festkörperforschung, Kernforschungsanlage Jülich,
Federal Republic of Germany

O. Hartmann, E. Karlsson and L.O. Norlin
Institute of Physics, University of Uppsala, Sweden

T.O. Niinikoski
CERN, Geneva, Switzerland

A. Yaouanc
CEN, Grenoble, France

(Submitted to Physical Review B)

ABSTRACT

In order to examine whether the small-polaron theory can describe the motional behaviour of light interstitials in metals at low temperatures correctly, we have systematically investigated the diffusion of positive muons in Al and in Al doped with substitutional impurities of various concentrations in the temperature range between 30 mK and 100 K. In pure Al (< 1 ppm overall impurity content) the muon was found to be mobile down to 30 mK. For doped Al, the diffusional behaviour exhibits two regimes: i) Above 1 K maxima in the depolarization rate evolve, indicating a static muon in the peak regions. The position of the peaks (between 15 and 50 K) is characteristic for each kind of impurity, while the height and width depend on the impurity concentration. In $\underline{\text{Al}}\text{Mn}_x$ the muon occupies a tetrahedral site in this regime. ii) Below 1 K the depolarization increases again with decreasing temperature and increasing impurity concentration. The temperature dependence exhibits a universal behaviour independent of impurity concentration and the kind of impurity. Here the muon site is octahedral. Both regimes are interpreted in terms of diffusion-limited trapping at the impurities: i) Above 1 K the diffusion is phonon-assisted and entails capture rates which increase with concentration and temperature. The peak positions are determined by the escape processes from the traps which occur at characteristic temperatures for each impurity. A quantitative analysis with a two-state model for diffusion in the presence of traps reveals a linear concentration dependence of the trapping rate. A linear temperature dependence for the diffusion coefficient is also found which is in strong disagreement with the T^7 prediction of conventional small-polaron theory. This linear behaviour is characteristic for a one-phonon process, which should be effective only if alternating transitions between octahedral and tetrahedral sites occur. ii) Below 1 K, the apparent trapping rate increases with decreasing temperature, implying a faster diffusion mechanism at low temperatures. The most appealing interpretation is a trapping preceded by a fast coherent diffusion, which is limited by muon-electron scattering. Again, in contrast to conventional small-polaron theory, which predicts $D_{coh} \propto T^{-9}$, we find proportionality to $T^{-0.6}$ for this rate.

1. INTRODUCTION

The diffusion of positive muons in metals has been studied intensively since the first pioneering work by Gurevich et al.[1] in 1972. It has been reviewed at two topical conferences held in 1978 [2] and 1980 [3], but several important problems still remain unresolved, in particular concerning diffusion in the presence of trapping centres and diffusion at very low temperatures. One reason for the continuous interest in these phenomena is that the muon diffusion rates have turned out to be extremely sensitive to various imperfections in the metals; another is that one can expect specific diffusion mechanisms, based on tunnelling, if the material is sufficiently clean and the thermal vibrations strongly reduced. At somewhat higher temperatures the muon diffusion should be similar to that of hydrogen isotopes (except for isotope effects), which evokes hopes of using the muon as a hydrogen substitute for studying diffusion, localization, and electronic structure in the very dilute limit.

Aluminium was one of the first metals which was subject to muon diffusion studies, since it is an fcc metal with large nuclear dipole moments. In fact, the depolarization rate (or line width) σ arising from the dipole broadening should be very similar to that of copper, where Gurevich et al. found $\sigma = 0.25\ \mu s^{-1}$, and a motional narrowing setting in above 100 K [1]. It was soon found, however, that pure Al gives rise to practically no depolarization of positive muons in the whole temperature range from 1-300 K [4].

The present work deals with positive muon diffusion and localization in the purest available aluminium and in aluminium doped with small amounts (usually 5-100 ppm) of specifically selected impurities: Mn, Mg, Li, Ag. There have been indications[5,6] that these isolated impurities will trap muons which are implanted at random in a sample, if the temperature is sufficiently high (10-50 K) for diffusion towards such impurity centres. These phenomena are now studied systematically for the first time, by variation of the impurity content of well-characterized Al samples. The aim is to find out which diffusion mechanism is dominant in the 0.1-10 K range.

It was shown in an earlier paper by our group[7] that a strong motional narrowing of the muon-spin rotation (μSR) signal occurs in the purest Al samples even if the temperature is as low as 0.03 K. This work has now been extended by including more accurate and systematic data from the same set of $\underline{Al}Mn_x$ alloys (x = 5, 10, 42, 57, 70 ppm) as mentioned above, from $\underline{Al}Li_x$ (x = 75 ppm), and from $\underline{Al}Ag_x$ (x = 117 ppm). These impurities were selected because they are expected to provide widely different long-range effects in the host lattice; Mn impurities producing a large volume change per atom and Li or Ag impurities giving nearly no such effects. The improved quality and the systematic nature of the new data should provide a basis for a discussion of those diffusion mechanisms which remain possible at very low temperatures, in particular the question of the existence of coherent diffusion. The diffusion data have been complemented by lattice-site determinations for muons, both at the lowest temperatures (≈ 50 mK) and in the trapping peak (at 15 K) for $\underline{Al}Mn_x$.

In Section 2 first the formation of small-polaron states of the muon is discussed and then the current theories of motion of a muon -- coherent and incoherent diffusion in ideal and non-ideal crystals, and trapping -- are reviewed. We have felt it necessary to make this review fairly extensive in order to define the problems and to see to what extent they can be put to experimental test. In Section 3 the experimental procedures are described and the results of our investigations on the diffusion of muons presented. Section 4 contains the experiments on the site determinations. The results are further discussed and compared with theory in Section 5. The conclusions are summarized in Section 6.

2. THEORY OF MUON MOTION

2.1 Small-polaron formation

In most theoretical discussions of the motion of muons in metals the muon is assumed to self-trap immediately after thermalization. Recently, however, questions on the polaron formation and a possible delay of it have been raised. Therefore, in this section we shall briefly discuss the theoretical approaches to the self-trapping process.

If a positively charged muon is implanted in a solid, thermalization occurs on a very short time scale[8]. In this process the muon will be screened by the conduction electrons of the metal, just like the proton. There remains a strong residual interaction with the host atoms mediated by the screening cloud. This interaction is often described in terms of lattice theory, where the short-range interaction is modelled by so-called Kanzaki forces $\vec{\psi}^m$ acting on the surrounding host atoms designated by the indices m. The strength of the elastic interaction between the muon and the host lattice can be parametrized in terms of the double force tensor $P_{\mu\nu}$, which is the first moment of the Kanzaki forces,

$$P_{\mu\nu} = -\sum_m \psi_\mu^m R_\nu^m \ , \tag{1}$$

where R_ν^m is the νth component of a vector from the muon to the host atom m. In a cubic system the trace of $\underset{\sim}{P}$ is related to the volume expansion created by the lattice relaxation around a self-trapped muon by

$$\Delta V = \frac{\mathrm{Tr}\ (\underset{\sim}{P})}{c_{11} + 2c_{12}} \ , \tag{2}$$

where c_{11} and c_{12} are elastic constants of the host metal. The elastic interaction favours self-trapping and small-polaron formation. For an isotropic elastic continuum the energy gain as a result of the lattice relaxation around the interstitial muon amounts to

$$\Delta U = -\frac{1}{2\Omega}\frac{P^2}{c_{11}} \ , \tag{3}$$

where P is the diagonal element of $\underset{\sim}{P}$ and Ω the volume of the primitive unit cell. With P = 1.42 eV (see Subsection 2.3) a value of ΔU = -86 meV is estimated for Al. Localization, however, also increases the kinetic energy of the muon, since higher Fourier components are involved in a localized state as compared to a long-wavelength plane wave.

For the case of the positron the balance between kinetic energy and potential energy has been investigated quantitatively in the framework of continuum theory as well as of harmonic lattice theory. Both approaches lead to a kinetic-energy contribution up to one order of magnitude too large to allow self-trapping. On the other hand, since the kinetic energy varies as m^{-1}, while the elastic energy depends only weakly on m, for the muon as well as for the proton the ground state should be the small-polaron state.

The next problem we have to tackle is the question: how does the muon, which initially starts in a non-self-trapped, delocalized state, reach its equilibrium state? For the adiabatic limit, where the light particle always immediately adjusts itself to the strain pattern of the lattice, Emin[9,10] investigated the existence of a barrier to self-trapping using scaling arguments. Following his method one can write the energy of a particle added to an elastic continuum as a function of a scaled position variable with scaling factor R. Three components contribute: i) the kinetic energy which scales as T_e/R, ii) the elastic potential energy of the particle which behaves as $-V_{int}/R^3$, and finally, iii) the resulting strain energy of the deformed continuum, which is given by $V_{int}/2R^3$. Thus, the total energy of the particle, which scales as

$$E(R) = T_e/R^2 - V_{int}/2R^3 \ , \qquad (4)$$

exhibits always a maximum for finite R. Both an infinitely spread-out muon as well as the small polaron, which in a discrete system shrinks to typical interatomic distances, appear to be possible and are separated by a barrier. Similar results have also been obtained by Browne and Stoneham[11], using a slightly different argument. In the context of scaling it can easily be seen that impurities which interact elastically with the muon (interaction potential $-V_{int}^{imp}/R^3$) reduce the barrier height.

In order to see whether the barrier causes any delay in self-trapping, the dynamic stability of the metastable non-self-trapped (free) state has to be investigated. Qualitatively it is clear that the ratio of the muon passage time in the

free state, characterized by the corresponding tunnelling matrix element J_f , to the reaction time of the lattice measured by the vibrational frequencies ω_D of the host lattice, will be the important parameter which describes the degree of adiabaticity A. For small $A = zJ_f/\hbar\omega_D$ (where z is the coordination number of the muon) the lattice can react and the muon will be self-trapped within a vibrational period $\sim 10^{-12}$ s, while for large A self-trapping will become increasingly difficult. This simple qualitative picture is supported by detailed variational studies of an electron in a deformable medium beyond the adiabatic limit[9]. In addition to the role of the adiabaticity parameter these calculations show that for a given A the free and the polaron state can only coexist within a certain range of $|\Delta U|\hbar\omega_D$. In order to judge the significance of a possible delay in self-trapping for the muon, the rigid lattice bandwidth has to be estimated. Taking the muon as a free particle, in analogy to a nearly free electron in a periodic lattice, a bandwidth in Al of about 30 meV can be evaluated, which is of the same magnitude as the typical lattice frequencies. Thus A is about unity and we are confronted with a border-line situation, where the theory cannot predict whether or not any delay in self-trapping will occur.

With respect to the actual experiments, the influence of temperature on the self-trapping mechanism is of great interest. Here it is useful to follow the picture given by Browne and Stoneham[11] of a critical fluctuation q_c of the host atoms above which localization occurs. For a single oscillator the probability that its vibrational coordinate exceeds a certain value q_c is given by

$$p_T(q > q_c) = \mathrm{erfc}\ (q_c/\tilde{q}) \ , \tag{5}$$

where $\tilde{q} = \hbar/2M\omega \coth (\hbar\omega/2k_BT)$. Expressing q_c by the bandwidth zJ_f and the coupling energy ΔU one finds

$$p_T(q > q_c) = \mathrm{erfc}\left(\frac{zJ_f}{\sqrt{\Delta U \hbar\omega \coth (\hbar\omega/k_BT)}} \right) . \tag{6}$$

Equation (6) shows again that a delay in self-trapping can only be expected for bandwidths of the order of, or larger than, typical lattice frequencies $\hbar\omega_D$. In addition, an influence of temperature can only be expected for thermal energies $k_B T$ of the order of $\hbar\omega_D$. This basic result does not change if one considers the strains arising from the distribution of thermal phonons in a crystal. For example, for Al metal, Browne and Stoneham estimated a 14% increase of the thermal strain energy between T = 0 and room temperature. Hence, thermal fluctuations are unlikely to provide temperature-dependent formation mechanisms at low temperatures.

We summarize the theoretical results concerning polaron formation as follows:

i) It is generally agreed that self-trapping of the positron does not occur.

ii) Using the derivations leading to (i) as a basis, it follows that for heavier interstitials, like the μ^+ or the proton, the polaronic state is the state of lowest energy.

iii) While protons always do occupy this state, in the case of the muon its lifetime of 2.2 μs may be less than a possible delay in self-trapping.

iv) Self-trapping is enhanced by phonon fluctuations and by impurities or lattice defects which tend to preform self-trapping distortions. The temperature influence is expected to be weak for T smaller than the Debye temperature Θ_D.

We conclude with a remark concerning the interstitial sites occupied by muons after a small-polaron state has formed. Some theoretical calculations for muons in Al [12-14] suggest preference of the octahedral (O) sites, compared to the tetrahedral (T) sites. These results, however, are very sensitive to the pseudopotential used. Channelling experiments[15-17] have indicated the T-sites as equilibrium positions of D in Al, but this result might be due to radiation damage. In our previous study[5] we have found the T-site in $\underline{\text{Al}}\text{Mn}_{0.0013}$ at 15 K.

2.2 Tunnelling and coherent diffusion

2.2.1 Tunnelling of small polarons

We assume that the muon has formed a small polaron in an ideal metal crystal, i.e. it is surrounded by a locally relaxed lattice. This small polaron can still

tunnel to a neighbouring interstitial site, which is related to the first site by a lattice translation. The tunnelling matrix element J_{eff} of this process comprises the transfer element J of the muon in the rigid lattice and the transfer of the relaxed lattice configuration between both sites. In the strong-coupling situation $|\Delta U| >> J$, which applies to Al, the effective tunnelling matrix element is obtained in the form

$$J_{eff} = J \exp\left[-S(T)\right] . \tag{7}$$

S(T) is determined by the Kanzaki forces ψ_{μ}^{m} and the lattice force constants, in the linear coupling approximation and for harmonic lattices. For simple estimates valid for isotropic solids the Debye approximation of S(0) is sufficient[18]

$$S(0) = \frac{5E_a}{2\hbar\omega_D} . \tag{8}$$

The quantity E_a is the activation energy for incoherent hopping of small polarons (see Subsection 2.3), and ω_D is the Debye frequency. As will be detailed in Subsection 2.3, an indirect experimental determination gives E_a = 32 meV and J ≈ 1 meV for Al, whereas a theoretical estimate for E_a is 40 meV. With the value $\hbar\omega_D/k_B$ = 428 K for Al one obtains S(0) = 1.73 using the experimental E_a, or S(0) = 2.16 using the estimated E_a. Hence J is reduced at T = 0 by a factor of 0.18 or 0.12, respectively, and estimated to be of the order of 0.1 meV for Al. The temperature correction of S(T) behaves as $(k_BT/\hbar\omega_D)^2$ for small T; hence it is of no interest at low temperatures.

The possibility of tunnelling transfer allows quantum-mechanical delocalization of a proton or muon such that in an ideal crystal at T = 0 the proton, or a long-lived muon, would be found in an extended state of Bloch type. The width of the corresponding "small-polaron band" would be roughly given by zJ_{eff}, where z is the coordination number of the lattice (z = 12 for the O-sites of the muon sublattice in the fcc lattice). However, this small-polaron band is rather hypothetical for muons, since there are always defects in a real crystal which provide isolated

localized states of low energy, i.e. which act as trapping centres. Ideally there is at most one muon in the sample at a given time, and it would always be trapped if it did not decay. The best one can hope for with respect to extended states is the formation of fairly extended wave packets of muons, which are unlikely to reach a trap during the muon lifetime in crystals with very small defect concentration. It is then necessary to discuss whether the formation of extended wave packets is possible at all in a crystal with defects, far from the isolated traps. This can be done by turning to the Anderson picture of localization.

According to Anderson[19] no band states exist in a non-ideal crystal when the average deviation ΔE of the ground-state energies of the interstitial sites exceeds a critical value E_c. For small-polaron bands $E_c \propto zJ_{eff}$; the exact proportionality factor is not well known for three-dimensional lattices[20]. We estimate, using elasticity theory, the deviations ΔE created by point defects in the regions far from the defects. We assume isotropic point defects in an anisotropic medium and use a formula given by Leibfried and Breuer[21], which represents an expansion in terms of the anisotropy c_a of the medium:

$$E_{int} = -\frac{1}{r^3}\frac{15}{8\pi}c_a\left(\frac{K}{\bar{c}_{11}}\right)^2 \Delta V^{\mu}\Delta V^{d}\left(\frac{3}{5} - \sum_j \rho_j^4\right) . \qquad (9)$$

Here $c_a = c_{11} - c_{12} - 2c_{44}$ is the anisotropy of the medium, $\bar{c}_{11} = c_{11} - \frac{2}{5}c_a$ is Voigt's average of c_{11}, $K = (c_{11} + 2c_{12})$ is the compressibility of the medium, ΔV^{μ} and ΔV^{d} are the volume dilatations produced by the muon and the defect, respectively, and ρ_j are direction cosines with respect to the cubic axis. For the estimate we omit the term containing ρ_j. We use $\Delta V^{\mu} = 2.9\ \text{Å}^3$, which has been found for hydrogen in fcc metals[22], and the elastic data of Al to obtain

$$\frac{dE_{int}}{dr} \approx 0.23\ \frac{\Delta V^{d}}{r^4}\left(\text{eV Å}^{-1}\right) . \qquad (10)$$

An estimate for the smallest value of ΔE is obtained by choosing r midway between the defects and multiplying by the distance d between interstitial sites. We use

$\Delta V^d = -7.4$ Å^3 for Mn; this value can be deduced from the measured lattice dilatation of Mn in Al [23]. We obtain from Eq. (10) $\Delta E \approx 1.6$ μeV for $\underline{Al}Mn_{50ppm}$ and $\Delta E \approx 0.12$ meV for $\underline{Al}Mn_{0.0013}$. The other impurities investigated produce similar (Mg) or considerably smaller (Li,Ag) lattice dilatations. The estimated lowest values for ΔE in the regions far from the defects in our samples are orders of magnitude smaller than the expected bandwidth of roughly 1 meV, except for Al with 1300 ppm Mn. Hence the transient formation of extended muon states appears possible at zero temperature in all the Al samples of our study, except in the one doped with 1300 ppm Mn.

In addition to the possible destruction of extended states by static disorder, also a dynamical destruction is possible by thermal vibrations. This mechanism is closely related to the transport in extended states to which we turn our attention now.

2.2.2 Coherent diffusion

We consider a muon which is self-trapped at a particular interstitial site. In the band picture and at zero temperature the wave packet would spread out over the crystal. At finite temperature, a finite mean free path ℓ of the wave packet results owing to scattering processes even in ideal crystals. The resulting diffusion coefficient can be represented, up to a numerical factor, as[24]

$$D \cong v^2 \tau \ , \tag{11}$$

where τ is an inverse (transport) scattering rate and v the velocity of the particle. While for electrons in metals v is equal to the Fermi velocity, for thermalized muons one expects v to be given by

$$v \approx (3kT/m^*)^{\frac{1}{2}} \ , \quad zJ_{eff} >> k_B T \ , \tag{12a}$$

$$v \approx dJ_{eff}/\hbar \ , \quad zJ_{eff} << k_B T \ , \tag{12b}$$

where d is the distance between two interstitial sites and m^* is the effective mass of the muon. With $J_{eff} \approx 0.1$ meV one expects the first equation (12a) to hold for

muons in Al well below 10 K. The mean free path of a wave packet is given by $\ell = v\tau$; this is also a measure for the coherence length of the wave packet. The region of transport in extended states, which is limited by scattering events, is commonly called "coherent diffusion".

Starting from the Liouville - von Neumann equation, Kagan and Klinger[25] have derived a diffusion coefficient of the form of Eq. (11), with $v \propto J_{eff}$ corresponding to the case of Eq. (12b). They assumed from the outset that J_{eff} is the smallest parameter of the problem, and that the diffusing particle is effectively localized (see below). They derived τ from an indirect phonon-scattering process, where the localized interstitial particle is in a virtual excited state between absorption and emission of the phonons, and found proportionality with T^{-9}. One of the present authors[26] has calculated τ from the direct phonon-scattering process on the localized interstitial particle. Also a T^{-9} behaviour was found and the prefactor was expressed in terms of the change of the elastic constants by adding interstitials. The relation $\tau \propto T^{-9}$ implies $D \propto T^{-9}$ for $zJ_{eff} \ll k_B T$ and $D \propto T^{-8}$ for $zJ_{eff} \gg k_B T$. If the dominating phonon interaction is the one with the fluctuating tunnelling transfer, D becomes proportional to T^{-7} or T^{-6}, respectively.

An interaction process neglected so far [see however Andreev and Lifshitz[27]] is provided by the scattering of electrons on the muons. This scattering rate should be proportional to the number of thermally excited electrons, i.e. proportional to T/T_F. Hence electron scattering should dominate at sufficiently low temperatures. The resulting diffusion constant should be proportional to T^{-1}, as suggested in Ref. 27, or be constant, depending on whether zJ_{eff} is smaller or larger than $k_B T$. Estimates of the muon-electron cross-section on the basis of a Thomas-Fermi approximation lead to a scattering rate of $\tau_{el}^{-1} \sim 10^{11}$ (T/K) s^{-1}. However, one should emphasize that this estimate does not properly take into account the directional dependence of the scattering events, as required for a transport scattering rate.

Scattering of wave packets on isolated defects is also possible. This process can only be dominant if other scattering processes are small, i.e. when the

mean free path in the absence of scattering centres is sufficiently large. One then expects a scattering rate $(\tau_d)^{-1} = v\sigma_{scatt}c$, where σ_{scatt} is the scattering cross-section and c the concentration of defects. For large mean free paths, the effect of the large de Broglie wavelength λ of the muon at low temperatures must also be taken into account. One estimates $\lambda \approx 25\ (T/K)^{-\frac{1}{2}}$ Å for a muon with an effective mass equal to the mass of the proton. For large λ the scattering cross-section will be proportional to v^{-1}, and the scattering rate will be independent of temperature even in the case where $zJ_{eff} >> k_BT$; see Eq. (12a).

If τ decreases with increasing temperature one reaches readily the temperatures where the mean free path ℓ is as short as the de Broglie wavelength λ of the muon at that temperature, or as the distance d between interstitial sites. The former case is relevant when Eq. (12a) applies, the latter when Eq. (12b) holds. According to Ioffe and Regel[28], the picture of transport in extended states is no longer applicable for $\ell < \max(\lambda,d)$. Especially when ℓ becomes equal to d, the particle has to be considered as localized. Kagan and Klinger[25] maintain that in a temperature region above that point, as long as J_{eff} is small, and thus the incoherent hopping rate negligible, the diffusion coefficient is still given by Eqs. (11) and (12b).

2.3 Incoherent hopping of small polarons

The coherent diffusion studied in the last subsection generally decreases with increasing temperatures; hence it will become small for larger T. At the same time, when ℓ becomes of the order of d, the muon is essentially localized at interstitial sites. A motion of a localized muon from one to a neighbouring interstitial site can now be induced by absorption (and emission) of thermal phonons. This leads to thermally assisted processes, called incoherent hopping.

2.3.1 Hopping in an ideal crystal

Small-polaron theory[18,29] predicts the following transition rate Γ between two neighbouring, equivalent interstitial sites:

i) At low temperatures when $k_BT << \hbar\omega_D$, Γ is proportional to T^7, see Ref. 29.

One finds for an isotropic solid

$$\Gamma = \frac{20\zeta(4)}{\pi^3} = \frac{P^4 d^4}{\rho^2 \hbar^{11} c_0^{14}} \; J_{eff}^2 (k_B T)^7 \; , \tag{13}$$

where ρ is the mass density of the host metal and c_0 the velocity of longitudinal sound. The factors in front of $J_{eff}^2 (k_B T)^7$ can also be expressed in terms of E_a and the Debye temperature Θ_D in analogy with Eq. (14) below. The temperature dependence is due to a two-phonon process, since in the ideal crystal a small polaron cannot absorb or emit a single phonon because of energy and momentum conservation. However, it can virtually absorb a phonon, tunnel to the neighbouring site, and then emit the phonon, with the rate given by Eq. (13). Fujii[30] has obtained a T^3 behaviour of the two-phonon contribution to Γ in the case of several non-equivalent interstitial sites in the unit cell.

ii) At higher temperatures when $k_B T \lesssim \hbar\omega_D$ one has

$$\Gamma = \left(\frac{\pi}{4 E_a k_B T} \right)^{\frac{1}{2}} \frac{J^2}{\hbar} \exp\left(- \frac{E_a}{k_B T} \right) . \tag{14}$$

A multiphonon process is necessary in order to bring the ground-state level of the occupied interstitial site to the same energy as the adjacent level. This requires the activation energy E_a. The particle can then tunnel with the transfer matrix element J; the golden rule yields the factor J^2 in Eq. (14). The remaining factor can be understood from the detailed dynamics of the coincidence of both levels[18].

It is difficult to estimate the parameters J and E_a with any accuracy from the existing pseudopotential calculations for Al. An estimation of J would require a precise knowledge of the potential energy curve of the proton or muon along its diffusion path. A derivation of E_a requires at least the knowledge of the Kanzaki forces between the proton or muon and the host atoms, and the force constants between the host atoms. Teichler[31] has calculated the small-polaron transition rate between O-sites in an fcc lattice in a model with one spring constant f, and the force g between a proton or muon and the nearest host atoms. He found

$$E_a = 0.26 \; g^2/f \; . \tag{15}$$

Unfortunately hydrogen is not soluble in Al, but g can be estimated for protons from the empirical volume expansion by hydrogen loading[23], giving approximately $ga = 1.42$ eV where a is the lattice constant. In the case of Cu, one obtains $ga = 2.46$ eV which compares well with the value of 2.64 eV deduced by Teichler[31] from diffusion data of muons in Cu. Hence we will adopt the value given above for the further estimates. Also the lattice expansion inferred from the values of the static line width (see Section 4) shows that ΔV produced by a muon is of the same order in Cu [32] and AlMn [5]. The spring constant f for Al determined from c_{44} is approximately 1.277×10^4 erg cm^{-2}. One obtains a value of $E_a = 40$ meV for muons from Eq. (15). This is an estimate for the activation energy of the muon diffusion, provided that the small-polaron hopping process is effective between octahedral sites in the fcc lattice.

So far thermally activated hopping of muons in pure Al has not been observed directly as a change of the depolarization rate with temperature; it seems to be too rapid in the temperature range of interest. Hence no direct experimental determination of J by application of small-polaron theory has been possible, contrary to the case of Cu [31]. An indirect estimate of J has become possible by the observation of muon trapping in vacancies in Al by Herlach et al.[33,34] at higher temperatures. Assuming diffusion-limited trapping they could verify the validity of Eq. (14) with $E_a = 32$ meV, which is in fair agreement with the estimate given above. Using Eq. (19) for the rate of diffusion-limited trapping we have estimated the prefactor of Eq. (14) from their data, and found J to be of the order of 1 meV. This is a fairly large value compared to the one for muons in Cu, where $J \approx 18$ μeV has been obtained[31].

2.3.2 Hopping in a non-ideal crystal

In a non-ideal crystal with defects the exact lattice translation invariance has been destroyed and the sites are no longer equivalent. Apart from the fact that defects provide trapping centres (to be studied in Subsection 2.4) there are energy differences ΔE between neighbouring sites even far from the defects. These differences have been estimated in Subsection 2.2. Here one-phonon processes can contribute to the transport since such energy differences allow absorption or emission

of single phonons. The transition rate between two sites with energy differences ΔE and transfer matrix element J was first derived by Sussmann[35]. Some modifications are necessary in order to include small-polaron effects; the corresponding transition rate has been deduced by Teichler and Seeger[36]. Their result contains contributions from even and odd combinations of the double force tensors of the muon in its initial and final state. For diffusion between equivalent sites only the even combination contributes and after applying an isotropic Debye approximation their Eq. (9) yields for *phonon absorption* ($\Delta E > 0$)

$$\Gamma_{abs} = \frac{J_{eff}^2 P^2 (\Delta E)^2 d^2}{6\pi\rho\hbar^6 c_0^7} \frac{\Delta E}{\exp\,(\Delta E/k_B T) - 1} \quad . \tag{16}$$

For *phonon emission*, ΔE has to be replaced by $|\Delta E|$ and the rate be multiplied by $\exp\,(|\Delta E|/k_B T)$. For $kT >> |\Delta E|$ one has

$$\Gamma_{abs} \approx \Gamma_{em} \approx \frac{J_{eff}^2 P^2 (\Delta E)^2 d^2}{6\pi\rho\hbar^6 c_0^7} k_B T \ , \tag{17}$$

i.e. a rate proportional to T. The rate equation (17) depends explicitly on the magnitude of the energy differences, contrary to the result found for reorientation of defects[37]. If the crystal is sufficiently pure, the contributions from Eqs. (16) and (17) will die out and one-phonon processes are only possible if odd combinations of the double force tensors $\underset{\sim}{P}_i$ and $\underset{\sim}{P}_j$ in the initial and final site contribute to the rate. They are non zero if the double force tensors are not the same in both sites. This can happen if the interstitial particle is diffusing between sites of different symmetry ($T \to 0 \to T \to 0 \to \ldots$) or if it is not located in the centres of the interstitial sites. The latter case appears to be very unlikely since the proton has always been found to be in a symmetry position in undisturbed metals. Starting from Teichler and Seeger's value and applying again an isotropic Debye approximation we obtain the one-phonon transition rate for this case in a high-T approximation ($\Delta\varepsilon << k_B T$ where $\Delta\varepsilon$ is now the energy difference between the two different interstitial sites):

$$\Gamma = \frac{J_{eff}^2 \left[\mathrm{Tr}(\underset{\sim}{P}_j) - \mathrm{Tr}(\underset{\sim}{P}_i)\right]^2}{2\pi\rho\hbar^4 c_0^5} k_B T \qquad (18)$$

plus a term which is equivalent to Eq. (17).

Although Eq. (18) does not contain $\Delta\varepsilon$ explicitly it is a consequence of an energetic difference between the sites considered. If equivalent sites of an ideal crystal are made non-equivalent by the introduction of defects, the difference of the traces in Eq. (18) would also depend on the strength of the disturbances.

2.4 Transition between coherent and incoherent diffusion: Summary

Assuming the theoretical expressions given above for coherent and incoherent diffusion, one can predict the transition temperature T_t below which coherent diffusion prevails and above which incoherent hopping dominates. If the same phonon interaction process would delimit coherent diffusion at lower temperatures and promote hopping at higher temperatures, T_t would coincide with the temperature above which extended states are no longer meaningful. The pertinent process is the interaction of the phonons with the effective tunnelling transfer. Holstein[24] has discussed in this way the temperature-dependent lifetime of band states and the concomitant transition to incoherent hopping. Also Petzinger[38] has developed a unified theory of coherent and incoherent diffusion; his predictions of T_t are some tenths of the Debye temperature of the host crystal. Additional interaction processes tend to further reduce coherent diffusion without promoting incoherent processes at higher temperatures; hence the actual transition temperature should be lower than estimated from the argument above. For example, Kagan and Klinger[25] have considered intrawell scattering of phonons on a localized interstitial, but they did not give an explicit prediction of T_t^{ph}. The rate derived from the direct phonon scattering process leads to an estimate of $T_t^{ph} = 34$ K in Cu [26] and similar values are expected for the other fcc metals.

Finally, taking into account electron-scattering processes we try to estimate the transition temperature from the Ioffe-Regel criterion. From the localization condition, mean free path equals lattice parameter, we get $v\tau \approx d$. Using the expression for the thermal velocity [Eq. (12a)] and an electron-scattering rate of $\tau^{-1} \approx 10^{11}$ (T/K) s^{-1} a transition temperature $T_t^{el} \approx 0.1$ K would result, which is more than two orders of magnitude smaller than the value predicted from small polaron theory.

To summarize, the main predictions of the theory of small-polaron motion in crystals are:

i) Diffusion occurs at low temperature through coherent transfer processes, resulting in a diffusion coefficient which in general increases with decreasing temperature.

ii) At higher temperatures diffusion takes place via thermally activated hopping of localized small polarons. The explicit behaviour with temperature depends on the process which is most effective in delimiting coherent transfer or promoting hopping. We have collected the various predictions for temperature dependences in Table 1. We emphasize that the ranges of validity are not included in the table; the main text should be consulted for their consideration.

2.5 Capture and release at trapping centres

It has been demonstrated by various experiments that defects can act as trapping centres for muons[39-41]; hence the motion of muons is strongly influenced by them. We will describe transport of muons in the presence of traps by a two-state model. In this model a particle spends an average time τ_1 in the state of diffusion; it it then captured by a trap, and released from the trap after a mean time τ_0. The implications of these processes on muon depolarization will be discussed in Subsection 3.5. In this section we will discuss in some more detail the parameters τ_0 and τ_1, of the two-state model. It is also possible to generalize the two-state model to an n-state model, in order to take into account several kinds of traps.

The escape out of a trap is only[42] possible by thermal activation; hence the escape rate τ_0^{-1} must exhibit this feature. The activation energy should be characteristic for the detailed structure of the trapping centre, i.e. specific for the kind of defect or impurity introduced. The escape rate τ_0^{-1} should be independent of the concentration of the trapping centres, except for secondary influences at higher concentrations. For structured traps the final escape results from several steps, and no simple relation between the total activation energy and that required for the individual steps is expected.

The capture rate τ_1^{-1} is sensitive to the nature of the transport processes which lead a muon towards a trapping centre. In the case of *hopping of localized muons*, the theory of diffusion-controlled trapping[43] can be applied, with the result

$$\tau_1^{-1} = 4\pi r_t D n_t \ . \tag{19}$$

Here r_t is the trapping radius and n_t the number of trapping centres per unit volume. Equation (19) is valid for a random walk with mean free path $\ell \ll r_t$. In the case of random walk on a regular lattice with randomly distributed traps a similar result holds. In the case of extended traps, r_t is an effective radius determined by the condition that the lowering of the saddle-point energies is approximately equal to $k_B T$, leading to [44] $r_t \propto T^{-1/3}$.

In the case of *coherent transport*, when $\ell \gg r_t$, the capture rate is given by[45]

$$\tau_1^{-1} = \sigma v n_t \ , \tag{20}$$

where v is the mean velocity of the muon, and σ the absorption cross-section. For sufficiently long mean free path, also the large de Broglie wavelength λ of the muon at temperatures below 1 K must be taken into account (see Subsection 2.2.2). For large λ and deep traps the absorption cross-section σ is proportional to v^{-1}; thus τ_1^{-1} becomes independent of v [45]. The result is a temperature-independent capture rate, as has been found for positrons trapped by vacancies[46]. Positrons

have a much smaller mass than the muons; however, the temperature of our investigations is much lower than in a typical positron experiment, hence similar conditions with respect to λ should hold. For shallower traps the effective absorption cross-section can depend on temperature in a complicated way. The behaviour of the capture rate in the intermediate region where $\ell \approx r_t$ is not well understood; one expects a smooth interpolation between Eqs. (19) and (20).

3. EXPERIMENTS ON MUON DIFFUSION

3.1 Preparation of samples

Because the dynamics of muons depends very sensitively on chemical and structural imperfections, high-quality samples are needed to obtain reliable experimental results. In the following the techniques used to prepare and to characterize such samples for the present investigations will be described.

Aluminium with less than one ppm of metallic impurities was used as base material (brand Kryal R-0Z from Vereinigte Aluminium Werke AG, Bonn). The residual resistivity ratio of this material varied between 15,000 and 30,000. The nominal purity of the alloying elements was: Ag (99.9999%), ^{7}Li (99.85%), Mg (99.998%), and Mn (99.99%). The alloys were prepared by HF-induction melting. To obtain homogeneous samples in the 100 at. ppm range an intermediate master alloy was used. The crucibles were made from high-purity alumina. Before melting the casting unit was evacuated to 10^{-5} Torr, flushed with argon, re-evacuated, and pressurized with 1400 Torr of an Ar+4% H_2 gas mixture. The melt was cast into graphite-coated stainless-steel moulds to form blocks with the dimensions 15 × 7 × 2 cm^3. From these blocks the polycrystalline samples (dimensions 3 × 3 × 2 cm^3) or the blanks for the single crystals were machined. Single crystals with a diameter of 1.3 or 1.5 cm were grown by the Bridgman technique. The material of the crucible was either graphite or boron nitride. (110)-oriented seeds were connected to the blanks by electron-beam welding. Crystals with a length of approximately 10 cm were grown at a rate of 0.5 cm/h. The atmosphere in the growth unit consisted of high-purity argon at a pressure of 1200 Torr, which was introduced into the apparatus after various pump-down cycles to 10^{-5} Torr. The crystals were usually

sectioned into three pieces by spark-cutting. After rechecking the orientation of each individual piece with X-rays, they were mounted on the sample holder.

Three techniques were employed to characterize the samples. The structural quality was assessed by diffractometry with 412 keV γ-rays. At every centimetre along the crystal axis the rocking curve due to a slice with a thickness of 0.1 cm was measured. Usually widths at half height below 30″ were obtained. In only a few cases they reached values of 120″. The concentration of the alloying element was determined by atomic absorption spectroscopy. From each individual piece of material up to three probes were taken and dissolved in HNO_3/HCl. At least three independent concentration determinations were made for each solution. The results are listed in Table 2. The level of residual impurities was checked by spark-source mass spectrometry. Probes were made by cutting a pair of pins from the bulk and by turning them on a lathe with a diamond tool. No etchant was used. Each pair of pins was analysed four times. The average results of some samples are reported in Table 3. The symbol < means well below. The reported values are considered to be on the high-level side. For the doping elements Ag, Li, Mg, and Mn the results obtained by atomic-absorption spectrometry are much more reliable. Because the mass spectrometer was adjusted for the high masses, a quantitative analysis of the Li line was not performed. The high carbon levels probably result from the use of the diamond tool. No figure is given for oxygen because the interference with the surface oxide was strong and erratic. The level of dissolved oxygen is estimated to be below 1 ppm. The high magnesium level may be correlated with the high vapour pressure of this element. The iron level in the AlMn sample is probably an artefact due to the reaction of an Mn^+ ion with the hydrogen of the residual gas atmosphere. A conservative conclusion is that the amount of all the residual impurities is less than 5 at. ppm and that the level of metallic impurities should not exceed 2 at. ppm. Finally one should keep in mind that the major part of these elements is segregated at structural sinks.

3.2 Experimental set-up

The experiments were performed in the muon beams at the 600 MeV Synchro-cyclotron at CERN, Geneva. Two different beam lines and experimental set-ups for μSR have been employed in this investigation. The CJ2 beam is the more intense, with typical count rates of ∿ 500 events/s. This figure is reached in spite of the fact that the effective detector solid angle must be limited to ∿ 15% because of the high positron contamination. The second beam line, the LJ1 beam, can give count rates of ∿ 300/s with a solid angle of ∿ 30%. This beam is much cleaner, with lower background, but can occasionally give problems with bad time structure.

In these experiments the detectors were normal plastic scintillators (NE 102) put together to make one in-beam muon sensitive telescope and two or three positron detector telescopes. In the positron-contaminated CJ2 beam a perspex Čerenkov detector was added to eliminate positrons by means of logical anticoincidences.

Ordinary leading-edge discriminators were employed for time definition since a time resolution of 3-4 ns is far from critical at the maximum magnetic field applied in these experiments (1500 G). Time histograms were collected by direct time-to-digital conversion at 500 MHz or 1 GHz clock frequency[47]. The number of events collected was varying from 1 to 3×10^6. In the more intense CJ2 beam a pile-up logic was always used to take away events where two muons were stopped in the sample within 10 μs. This reduced the rate of data collection by ∿ 30%. In the LJ1 beam pile-up rejection had no noticeable effect and was therefore sometimes omitted.

The CJ2 beam line is equipped with an iron magnet and a ^{4}He continuous flow cryostat capable of reaching temperatures down to 2 K. The lower temperature data were taken in the LJ1 beam in a ^{3}He-^{4}He dilution refrigerator, which can cool the μSR samples to 30 mK; the maximum temperature that can be stabilized accurately in this set-up is around 15 K. Therefore some overlap of the temperature ranges is possible. The magnetic field in the LJ1 beam is given by a Helmholtz coil. At present the maximum field is limited to 1400 G, which however is enough to essentially decouple the electric field gradient on the Al nuclei in the AlMn alloys.

The temperature was measured with calibrated germanium, carbon, and platinum resistors, and was stabilized within 0.2-1.0%. In the dilution refrigerator problems arise below 100 mK, since our calibrated Ge resistor attached directly to the sample lost heat contact below that temperature. On the other hand, carbon resistors were sensitive to beam heating in this temperature range. Reproducible results for the lowest temperatures could best be obtained by reading a carbon resistor placed on the sample holder a few centimetres out of the central beam spot. It was quite clear that the holder and sample were in good thermal contact, since the measured μSR damping parameter responds to holder temperature changes all the way down to the lowest temperatures. Also, in the absence of beam a carbon resistor attached to the sample showed temperatures compatible with that of the holder. The low temperature measurements on the $\underline{\text{Al}}\text{Mn}_{5\text{ppm}}$ sample were unfortunately made with a reversed resistor arrangement, and the derived temperatures are in this case based on comparisons with a third resistor placed far away from the sample. Above 100 mK no such problems were found.

The orientation of the single crystals was checked with Laue back-scattering after the mounting on the sample holders. The accuracy of the orientation, including the mounting in the cryostats is 2-3°. In the ^{4}He cryostat the samples can be rotated around an axis perpendicular to the magnetic field and the beam direction. Thus it is possible by mounting the single crystals with the (110)-direction parallel to the axis of rotation (for cubic lattices) to turn any of the main crystal directions (100), (110), or (111) parallel to the direction of the magnetic field. In the dilution refrigerator this rotation is not possible, and the single-crystal samples had to be taken out and reoriented on the sample holder.

3.3 Data treatment

Transverse-field muon-precession data are normally analysed with the expression

$$N = N_0 \exp(-t/t_\mu) \left[1 + a_0 P(t) \cos(\omega t + \phi)\right] + Bg \ , \qquad (21)$$

where $t_\mu = 2.20$ μs is the mean lifetime of the muon, ω is the precession frequency with initial amplitude a_0, and Bg is the accidental (flat) background. The damping

of the polarization P(t) is typically taken as either exponential exp $(-\lambda t)$ or Gaussian exp $(-\sigma^2 t^2)$. In practice a more complete expression is always used at CERN:

$$N = N_0 \exp(-t/t_\mu) \left\{1 + \left[a_0' P(t) + b_0 f_b(t)\right] \cos(\omega t + \phi)\right\} + Bg \ . \qquad (22)$$

Here a_0' is the effectively observable asymmetry from the sample and b_0 is the asymmetry originating from muons stopping in regions around the sample (sample holder, cryostat walls, etc.). This fraction is never negligible in the CERN beams; b_0 is typically between 0.02 and 0.06, depending on sample size, etc., while the total observable asymmetry a_0 ranges from 0.18 to 0.26.

This precessing background component is characterized by an asymmetry b_0 and a damping function f_b, while the frequency can be taken as equal to that of the muons in the Al samples. Empirically it has been found that a Gaussian damping $f_b(t) = \exp(-\sigma_b^2 t^2)$ is a good representation of the background function. The parameters b_0 and σ_b were determined by replacing the actual sample by a dummy sample of stainless steel having the same dimensions and mass, in order to ensure the same absorption conditions as in the real measurements. The stainless steel becomes antiferromagnetic below 40 K, and no precession signal from the dummy sample can then be seen. Therefore the remaining precession signal gives the background from the surroundings, under similar conditions to those in the real measurements.

A complementary way to obtain information about the precessing background is to reduce the temperature to well below the superconducting transition temperature ($\sim$ 1 K), while keeping the Al samples in zero magnetic field. A weak magnetic field (below 100 G) is then turned on, and the small precession signal from the surroundings can be observed. This procedure will however only yield b_0 since σ_b is affected by the magnetic-field distortion around the superconducting sample. Since, however, σ_b is very well known for the LJ1 set-up, this procedure could be used in a few cases in order to save the time for sample changes, which takes about twelve hours in the dilution refrigerator.

3.4 Results of the measurements

As mentioned in the Introduction, pure Al does not show any measurable depolarization down to low temperatures. The temperature range has been extended by our group down to 30 mK [7,48] and the depolarization rate has been found negligible down to 100 mK. The low-temperature results for the damping parameter σ for pure Al have been included in Fig. 1.

The dramatic effects of doping Al with small amounts of impurities can be seen in Fig. 1. Here the depolarization rate σ is displayed for various contents of manganese impurities, and compared with the results from undoped Al. The damping parameter σ is used which follows from the assumption of Gaussian depolarization $P(t) = P_0 \exp(-\sigma^2 t^2)$. More details on the depolarization process can be found in Subsection 3.5.2. Values of σ below 0.05 μs^{-1} can hardly be distinguished from zero depolarization within the statistics of the measurements. The small increase in σ for the "6N" Al sample below 100 mK is however believed to be a real effect, presumably reflecting the influence of the residual $\sim$ 1 ppm impurities.

The temperature dependence as appearing in Fig. 1 can for convenience be separated into two different regions -- one below 1 K where σ is roughly proportional to ln (1/T), and another above 1 K where a characteristic peak in the depolarization rate appears. At still higher impurity concentrations the two regions are not as well separated, as can be seen from Fig. 2 where the results from a 1300 ppm sample is shown together with other single-crystal results. The 1300 ppm sample has been measured several times, and the data included in the figure contain several measurements with the field in the (111)-direction. In fact these data are in reality coming from two samples, one with 1137 ppm and the other with 1296 ppm of Mn, but since we do not find any significant difference in the μSR results we use 1300 ppm as a common notation.

The temperature and concentration dependence of σ in the region above 1 K shows the typical features of capture and release of muons from traps. Figure 3 shows this region in more detail for the AlMn samples of various concentrations. The 1300 ppm sample shows clear indications of saturation, i.e. around 15 K

practically all muons are staying in traps during the time of observation. In this sample a secondary peak seems to appear at higher temperatures. Similar extra peaks have been seen in other strongly doped Al and Nb samples[6,39,49].

The effect of doping Al with other kinds of impurity atoms can be seen in Fig. 4. In the region above 2 K this appears as a shift of the characteristic temperature for the trapping peak, i.e. the escape process starts around 20 K in AlMn and AlAg but around 50 K in AlLi and AlMg. The AlMg results should be compared with a measurement by Kossler et al., on an AlMg sample with higher concentration (1000 ppm)[6]. The characteristic escape temperature is the same, and even the indications of a double structure in the peak is similar, for the two different concentrations.

While the trapping peak appears at temperatures seemingly characteristic for each kind of impurity, the low-temperature data below 1 K are very similar for AlMn, AlLi, and AlAg. Figure 5 shows this part of the temperature range, and it is evident that the functional form of the temperature dependence is identical for the different impurities. The Mn atoms appear to produce a stronger depolarization per impurity atom than Li and Ag. This may be related to the local lattice distortion around the impurity, where Li and Ag act only locally giving practically zero net volume expansion.

3.5 Evaluation of results above 1 K

3.5.1 Depolarization through incoherent hopping, including trapping

As has been noted above, the measured depolarization parameter σ in the Al alloys above 1 K shows features which are characteristic of trapping and escape processes. In order to analyse the data further we need a relation between the observed depolarization and the hopping processes, including trapping. Since these topics have been covered in detail in several publications[39,50-53] we only indicate the main results of the theory.

An immobile, point-like muon shows in good approximation a Gaussian depolarization (normalized to unity).

$$P(t) = \exp\ (-\sigma^2 t^2)\ . \tag{23}$$

The width of the Gaussian σ is related to the dipolar interactions of the host atoms with the muon; see Subsection 4.1. If localized muons perform hopping motion, they are under the influence of different dipolar fields during their lifetime. The rotation frequency ω' of the transverse muon spin due to the dipolar fields becomes time-dependent. One usually assumes a Gaussian-Markovian process for $\omega'(t)$ with a correlation time τ_c, which should be proportional to the mean residence time of a muon on a particular site. The polarization decay resulting from this assumption is[54,55]

$$P(t) = \exp\left\{-2\sigma^2\tau_c^2\left[\exp\ (-t/\tau_c) - 1 + t/\tau_c\right]\right\}. \tag{24}$$

For $\sigma\tau_c \gg 1$, i.e. practically immobile muons, one obtains from this equation the static result of Eq. (23), whereas for $\sigma\tau_c \ll 1$, corresponding to rapid motion, one finds exponential decay which represents motional narrowing,

$$P(t) = \exp\ (-2\sigma^2\tau_c t)\ . \tag{25}$$

A "strong-collision" model, where ω' changes its values abruptly, leads essentially to the same results[51,55]. One of the authors[56] has numerically investigated the relation between the residence time τ and τ_c. It was found that τ is very close to τ_c for O- and T-sites in fcc lattices, while they can differ considerably for bcc lattices at high applied fields.

The influence of capture and release processes on the depolarization of the muon spin in the case of incoherent hopping can be treated in the framework of the two-state model outlined in Subsection 2.5. According to this model, a muon diffuses in a free state for a mean time τ_1, and then spends a mean time τ_0 in the trap, etc. This process is similar to the elementary processes of the strong-collision model, and that model is also easily extended to include trapping and detrapping[51,52]. The depolarization decay is determined by two coupled integral equations which can be solved explicitly in the Laplace domain. The solution for

P(t) in the time domain is then obtained by numerical transformation. Since this procedure is somewhat unwieldy for use in fitting routines we actually used the approximate treatment of the polarization decay within the two-state model by a set of two coupled differential equations[39]. As has been shown in Ref. 51, the solutions of the differential equations are always similar to the solutions of the integral equations; especially the resulting damping parameters of both approaches differ only slightly. Also other derivations of the polarization decay for diffusion in the presence of traps have been given; for example, Petzinger, Munjal and Zaremba[53] have developed a Gaussian-Markovian theory for P(t).

3.5.2 Results for the parameters

In order to obtain the physical parameters for the trapping region above 1 K we have fitted the data with the differential equations for the two-state model of Ref. 39. The fitting was actually done in two steps by first deriving a σ value from the theoretical P(t) function, and then comparing the experimental and theoretical σ values in a least-squares fit. Here we have used the value $\sigma_0 = 0.265\ \mu s^{-1}$ for the damping in the absence of motion when fitting the data taken in a 150 G magnetic field, while the $\underline{\text{Al}}\text{Mn}_{42\text{ppm}}$ sample measured at 500 G was fitted using $\sigma_0 = 0.22\ \mu s^{-1}$. In principle, a simultaneous fit of several measurements with the static σ as a free parameter could be attempted, but this has not been done with the present data.

The differential equations of Ref. 39 were solved on the assumption that the muon diffusion in the free state is rapid enough to give zero depolarization. In this case τ_c is very small and the equations of Ref. 39 can be simplified. The resulting systems of equations were solved by a Runge-Kutta method, and used in the least-squares fits to the experimental σ values. The temperature dependence of the escape rate was taken as an Arrhenius-type process $\tau_0^{-1} = \Gamma_0 \exp(E_a/k_B T)$, while the capture rate τ_1^{-1} appears almost proportional to T. In the fits we used $\tau_1^{-1} = \Gamma_1 T^{\alpha}$ with the exponent α as a free parameter, which was found to be slightly below one for the $\underline{\text{Al}}\text{Mn}$ samples. The data from three different concentrations were fitted simultaneously with a common temperature dependence but different prefactors. The results of the fit are found in Table 4.

The fitting of the trapping peaks in the case of the other impurities is complicated by the fine structure visible in the line width as a function of temperature, and the parameters summarized in Table 4 are to some extent an average description of the situation. A fit with several trapping centres as in Refs. 6 and 49 was not considered worth while.

3.6 Evaluation of results below 1 K

3.6.1 Depolarization through coherent motion

As mentioned in Section 2 there are reasons to believe that coherent processes may be effective below 1 K. We must therefore consider the interpretation of the depolarization in the region where coherent diffusion prevails. Although the theory of depolarization has only partially been worked out for this case, we try to outline the behaviour of $\sigma(T)$ for coherent diffusion, followed by trapping in impure crystals.

The polarization P(t) of the spin of the muons can be expressed in terms of the time-dependent correlation function of the magnetic fields acting on the muon[55,57]. Assuming that there is no reaction of the muons on the dipolar fields and that T_1 processes can be neglected, McMullen and Zaremba[57] showed that the decay rate of P(t) is determined by the "self-diffusion function" $\langle \hat{n}(\vec{r},t)\hat{n}(\vec{r}'t')\rangle$ where $\hat{n}(\vec{r},t)$ is the density operator of a muon at time t. For sufficiently long times the decay rate is governed by the correlation time τ_c defined by

$$\tau_c = \int_0^\infty d(t - t') \; \langle \hat{n}(\vec{r}t)\hat{n}(\vec{r}'t')\rangle \; . \tag{26}$$

For incoherent hopping τ_c is proportional to the mean residence time on a site. For coherent diffusion in the transition region to incoherent jumps, where the extension of the wave packets is still small, τ_c should be given by the effective time of transfer to a neighbouring site, i.e.

$$\tau_c \approx a^2/D_{coh} \; . \tag{27}$$

If $\tau_c \sigma << 1$, the polarization decay in this region should correspond to motional narrowing according to Eq. (25) with τ_c given by Eq. (27).

It is not clear at present how the theory should be extended to the region where coherent motion occurs with large mean-free path, i.e. to the region of very low temperatures. The case of ferromagnetic materials has been treated by Fujii and Uemura[58,59], but their results are specific for ferromagnets. Fortunately a complete theory of depolarization in the case of coherent diffusion is not required for the interpretation of the present experiments, as will be pointed out below.

The purest Al shows virtually complete absence of depolarization down to 100 mK; in other words there is practically no structure in $\sigma(T)$ which could be compared with theory. In order to deal with the impure samples, depolarization in the case of coherent diffusion in the presence of trapping centres must be considered explicitly. This can be done again in the framework of the two-state model. Here two simplifications can be made:

i) Complete motional narrowing can be assumed during the coherent diffusion of the muon in the undisturbed regions of the crystal, in view of the findings for pure Al.

ii) Release processes from the traps can be neglected at the temperatures considered, since they would require thermal activation.

Then, the main source of depolarization is the trapping of the muons, which is determined by the trapping rate $1/\tau_1$. Contrary to depolarization during the diffusion process, where the damping is proportional to τ_c [see Eq. (25)], it is now roughly proportional to $1/\tau_1$. This can be seen by taking the limit for "long" capture times ($\sigma_t \tau_1 >> 1$) in the coupled integral equations of Refs. 39 and 51.

3.6.2 Results

We have first fitted the experimental data below 1 K by the formula (24) which interpolates between Gaussian depolarization and motional narrowing but assumes a uniform type of motion over the time of observation. Figure 6 shows the inverse correlation times τ_c^{-1} for the different AlMn samples. In this double logarithmic

plot the results from a common fit of the 5, 10, 42, and 70 ppm samples are presented as solid lines. The best fit to the data is

$$\tau_c^{-1} = 6.9(1.2) \times T^{0.60(4)} c^{-0.76(4)} \times 10^5 \ s^{-1} \ , \tag{28}$$

where T is given in mK and c in ppm. The possible interpretations of such a straightforward application of Eq. (24) are discussed in Section 5.

As suggested above, we have also fitted the data by the two-state model. The differential equations of Ref. 39 were used and fast diffusion in the free state ($\tau_c^{-1} \to \infty$) together with negligible escape ($\tau_0^{-1} \to 0$) were assumed. The result of the fit of τ_1^{-1} is then

$$\tau_1^{-1} = 3.0(6) \times T^{-0.61(4)} c^{0.76(4)} \times 10^5 \ s^{-1} \ . \tag{29}$$

Compared with Eq. (28), τ_1^{-1} exhibits reversed signs of the exponents of T and c, as is expected from Subsection 3.6.1.

The fits in Eqs. (28) and (29) were made directly to the full depolarization function P(t). This is one of the reasons for the slightly different values of the exponential factors from those given in Ref. 48. The temperature scale has also been slightly corrected, especially for the 5 ppm sample, where the experimental uncertainty is large.

4. EXPERIMENTS ON SITE DETERMINATION

4.1 General remarks

Muon spin rotation offers the possibility of determining the symmetry of the interstitial site where the muon is located by investigating the dependence of the line width σ on magnetic field and crystal orientation. We consider immobile point-like muons which show Gaussian depolarization according to Eq. (23). The value of σ is determined by the dipolar fields created by the host metal atoms at the site of the muon. Van Vleck[60] has first evaluated the second moment of the distribution of dipolar fields in the context of NMR. His result as applied to muons is

$$\sigma^2 = \frac{1}{6}\gamma_\mu^2\gamma_H^2\hbar^2\, S(S+1)\sum_j \frac{(3\cos^2\theta_j - 1)^2}{r_j^6} \,. \qquad (30)$$

Here S is the spin of a host atom, γ_H its gyromagnetic ratio, r_j the distance between the muon and the host atom j, and θ_j the polar angle of the vector $\vec{r}_j$ with respect to the $\vec{B}$ axis.

For a single crystal, according to Eq. (30), σ depends on the orientation of the crystal with respect to $\vec{B}$. Values for σ in cubic metals are quite different for the main symmetry directions (100), (110), and (111), and depend strongly on the type of interstitial site. Hence a determination of the type of site is possible through the measurement of σ, by orienting the crystal in different symmetry directions. Hartmann[61] pointed out that this consideration only holds for large magnetic fields, since at small fields contributions of the electric field gradient created by the muon itself can come into play. As a charged impurity, the muon creates an electric field gradient (EFG) at the neighbouring host nuclei. When these nuclei have a quadrupole moment, a new quantization axis of the nuclear moments has to be determined from the combined magnetic and electric interactions. The result for the dipolar width σ depends strongly on the relative interaction strength $y = \omega_0/\omega_E$, where ω_E is an electric interaction frequency determined by the quadrupole moment and the strength of the EFG. For small y the EFG interaction dominates and σ is nearly isotropic; for $y \gg 1$ the van Vleck values in Eq. (30) are obtained. Al possesses a quadrupole moment Q = 0.15 barn, and the ratio of the quadrupole to magnetic moment is somewhat lower than in Cu. It should therefore be quite easy to quench the electric interaction by applying magnetic fields. The crossover from electric to magnetic field behaviour occurs around $y \approx 5$; for a detailed discussion see Ref. 61. The field dependence of the depolarization rate σ can also be used to estimate the strength of the EFG produced on the surrounding lattice nuclei.

4.2 Experimental results

The first measurement of the field dependence in Al was made on the 1300 ppm single-crystal sample. Here the puzzling fact emerged that at 15 K the muon site appears to be tetrahedral, while at lower temperatures (2-7 K) there seems to be a mixture of octahedral and tetrahedral interstitial sites[5]. Since then we have made several other measurements on single crystals and the present situation is illustrated in Fig. 7. The data indicate at the lowest temperatures a practically pure O-site, while the intermediate region is a mixture, and finally the trapping peak at 15 K has tetrahedral symmetry as before.

The absolute values of the σ's are smaller than the calculated values for point-like muons in undistorted environments. This effect is about 30% for the 1300 ppm sample at 15 K, where we believe that all muons are trapped and a static line width is observed. As in the case of Cu [32] this can be ascribed to either a local lattice dilatation ($\sim$ 10%) or a local spread of the muon wave function.

The quadrupole frequency $\omega_E/2\pi$ derived from the 1300 ppm sample at 15 K is 0.051 MHz. This corresponds to a field gradient of $q = 0.40$ Å^{-3} at nearest neighbours. The previous value given in Ref. 5 was numerically wrong by a factor of two. The uncertainty in the determination of ω_E is around 15%, and in addition errors in the quadrupole moment will affect the uncertainty in q.

The EFG at the lowest temperature was also derived from the 50 ppm data (O-sites). The value at nearest neighbours is 0.30 Å^{-3}. This somewhat lower value at the octahedral position could just reflect the increased muon-Al distance (an r^{-3} dependence assumed for q leads to a relative decrease of 0.65 compared to the T-site).

In the previous discussion we have assumed that the muon is in a pure Al dipole environment. This is certainly a good approximation for the AlMn samples, where the Mn atoms have about the same magnetic moment as the Al atoms. In addition, the field gradient created by Mn on neighbouring Al atoms is known to be 0.45 Å^{-3}.

Although the exact behaviour of the muon line width in this complicated situation with the two different sources of field gradients has not been calculated, we have previously drawn the conclusion that the muon can hardly be a nearest neighbour to the Mn atom.

We have also studied the magnetic field dependence of the $\underline{\text{Al}}\text{Mn}_{42\text{ppm}}$ polycrystal at 40 K. The measurement does not give as clear information as a single crystal, since the site cannot be determined and the maximal change in σ with B is only 32%. However the data indicate that the electric field gradient is somewhat smaller in $\underline{\text{Al}}$Mg at 40 K than in $\underline{\text{Al}}$Mn at 15 K. The reason for this is not clear -- a different site preference is a possibility. Experimental problems may also have influenced this measurement.

There is also the possibility that an electronic moment at the Mn atom contributes to the line width of the muon. It is not certain whether $\underline{\text{Al}}$Mn can be considered as a Kondo system. But if this is the case, the Kondo temperature is 700 K, which leads to spin fluctuations of the order of 10^{14} s^{-1}. This rapid fluctuation rate gives a negligible contribution to the depolarization (less than 0.001 μs^{-1}) even if the muon is at the nearest interstitial site to the Mn atom. Also the similarity of the depolarization rate in Fig. 5 obtained for $\underline{\text{Al}}$Ag and $\underline{\text{Al}}$Mn is evidence against any paramagnetic effects from the Mn.

5. INTERPRETATION

As was noted in the presentation of the results the observations fall naturally into two categories, reflecting essentially different processes above and below T = 1 K, respectively. The same division will be kept as we now attempt to interpret the data in somewhat more detail.

5.1 Region above 1 K

The salient features of muon depolarization in Al crystals with impurities above 1 K, can be summarized as follows:

i) There are maxima in the damping rate $\sigma(T)$,

ii) The heights of the maxima increase with the concentration of the impurities,

iii) The positions of the maxima and the detailed shape of $\sigma(T)$ are specific for each kind of impurity introduced.

These observations constitute clear evidence that muons, which diffuse by thermally activated processes at these temperatures, are captured and released by the impurities. Some points of this general picture need more detailed consideration.

The data for Mn-doped Al and the analysis by the two-state model show that the capture rate τ_1 is proportional to c. Hence the trapping takes place at single impurities (except for c = 1300 ppm as will be discussed below). The two-state model can also be used to extract some information on the nature of the traps. We consider Al with 70 ppm Mn as a particular example. At a temperature of 17 K, corresponding to the maximum of $\sigma(T)$, the fit by the two-state model gives $\tau_1 = 3.3$ μs and $\tau_0 = 40$ μs. Not every muon is caught by a trap during its lifetime in this sample at 17 K; however, when it is trapped it will rarely escape. The mean equilibrium population of traps corresponding to these values is 92%. Owing to the non-equilibrium initial conditions and the finite lifetime of the muons the actual average population of the trapping sites will be reduced to about 30% of this value).

On the other hand, if one estimates the mean equilibrium population for trapping sites with a binding energy corresponding to 120 K (see Section 3) from Boltzmann statistics, one finds a value of only 7.5% at 17 K for this sample. We ascribe this apparent discrepancy to the structure of the trapping centres. Each impurity creates a region containing several sites where muons are effectively caught. The comparison of the thermal and the two-state values of the populations suggests a factor of the order of 100 trapping sites for each Mn atom. Extended traps can also modify the activation energy for escape, i.e. the activation energy seen in the depolarization process can be smaller than the binding energy. Analogous effects have been observed in a neutron-scattering experiment on H in NbN_x [62]. In the sample with 1300 ppm Mn one finds almost no indication of motional narrowing below 17 K. This can also be attributed to the existence of extended regions around the Mn atoms, where the motion of the muons is strongly hindered.

Another experimental fact supporting the picture of extended traps is the value of the EFG derived for the muon sites at 15 K in the Mn-doped samples. It is characteristic for a T-site in a pure Al environment. It is therefore improbable that a Mn atom is a nearest neighbour. Herlach et al.[33,34] have studied the trapping of muons on vacancies in Al produced by electron irradiation and found no indications of trapping for 5 ppm vacancies in the temperature range under discussion, whereas for 5 ppm Mn clear indications of trapping are observed. We conclude that the trapping radius of Mn exceeds that of vacancies considerably.

The application of the theory of diffusion-limited trapping to the experimentally determined trapping rate leads to a diffusion constant nearly proportional to T, for temperatures between 1 K and the maximum of $\sigma(T)$. The fitted exponent of T in

$$\tau_1^{-1} \propto T^{\beta} \tag{31}$$

is $\beta = 0.89(3)$. This temperature dependence is in obvious disagreeement with the theoretical predictions for incoherent hopping, see Subsection 2.3, i.e. no T^7-behaviour is seen. On the other hand, it is in qualitative accordance with the rate expected from a one-phonon process. For the strain-induced part of the one-phonon process the diffusion rate is proportional to $(\Delta E)^2$, where ΔE is the energy difference between strain-split levels, see Eqs. (16) and (17). The average $(\Delta E)^2$ should increase with increasing impurity concentration proportional to c^2, according to a rough estimate. Practically no dependence on the concentration of impurities is seen in the hopping rate deduced from the capture rate, after the trivial concentration factor of Eq. (19) has been divided out. In addition, the jump rates should be very different for impurities with large and small long-range strain field. The data for the different impurities used in this study lead to quite similar jump rates, in contradiction to the expectation (see Table 4).

There remains the possibility of one-phonon induced transitions between crystallographically inequivalent sites, for instance transition sequences $0 \rightarrow T \rightarrow 0 \rightarrow T \rightarrow 0 \rightarrow T$ ... in the fcc lattice as described by Eq. (18). Such processes

would be independent of strain energy differences ΔE as long as $\Delta E \ll E_O - E_T = \Delta\varepsilon_{OT}$, and could give rise to a linear temperature dependence for $k_B T \gg \Delta\varepsilon_{OT}$.

A comparison between the trapping curves for impurities with different volume expansions (Mn and Mg on the one hand and Li and Ag on the other) shows only a partial correlation between the long-range strain field produced by an impurity and the capability of this impurity to trap (Fig. 4). The escape appears not to be correlated at all. The values of the volume expansion induced by these impurities have been given in Table 5 for comparison.

Neutron-diffraction experiments on Al doped with the same impurities have shown that short-range displacements of the host atoms exist also in the case of small or negligible long-range dilatations[63]. We conclude that the depths and radii of these trapping regions depend on the detailed electronic structure around each type of impurity and cannot be predicted from the long-range behaviour.

It is also impossible at present to extract direct information from the positions of the maxima of $\sigma(T)$, since they are determined by an interplay of capture and release processes which can be quite complicated for structured traps. The rise of $\sigma(T)$ to the trapping peaks shows secondary maxima for Li and Mg which might be caused by trapping at an intermediate shallow level, i.e. by the internal structure of the trap. The deviations from linear temperature dependences found for these samples may be due to the fact that such effects have not been taken into account.

5.2 Region below 1 K

From the analysis of muon depolarization in pure Al and the Al alloys the following facts have emerged:

i) $\tau_c \propto c^{0.76}$.

ii) $\tau_c \propto T^{-0.6}$.

iii) Impurities with small (Li) or negligible (Ag) volume dilatations give rise to the same depolarization (apart from a small quantitative factor) as the impurity with large volume dilatation (Mn).

iv) The muons occupy O-sites at the lowest temperature in contrast to the T-sites found at high temperature (15 K) for the same Mn-doped samples.

v) The muon is localized at or near one single interstitial site, for most of its lifetime, as deduced from the EFG, at least in $\underline{\text{Al}}\text{Mn}_{50\text{ppm}}$ at the lowest temperatures.

We cannot offer a unique and simple explanation of all facts noted above. Instead we will discuss different possible explanations and try to deduce the most likely one.

We will first examine whether the observed facts can be understood from motional processes in the bulk material which do not change their character during the lifetime of the muons, i.e. we disregard trapping.

We first consider *uniform incoherent motion* of the muons down to the lowest temperatures. The rise of $\sigma(T)$ with $T \to 0$ would then be caused by the gradual freezing of this process. A candidate is the apparent one-phonon process whose existence was supported by the $T > 1$ K data. The T-dependence is in qualitative, but not quantitative, agreement with such a model which would predict $\tau_c^{-1} \propto T$ (for $|\Delta E| \ll k_B T$). The strain-induced part of this mechanism would however produce an increased jump rate (decrease of σ) with increasing c contrary to the reversed dependence on c (i). The rate for jumps between O- and T-sites would be independent of c at these low concentrations. Both possibilities can therefore be discarded. Since the motion process should take place mainly in regions relatively far from the impurities where Eq. (9) should be valid, it would also be difficult to explain the independence of the kind of impurity (iii) in this context.

Secondly, we discuss whether the rise of $\sigma(T)$ as $T \to 0$ might be due to *uniform coherent motion*. According to the discussion of polarization decay in the case of coherent diffusion in Subsection 3.6, the correlation time should be inversely proportional to D_{coh}, see Eq. (27). The result for τ_c would then imply $D_{coh} \propto c^{-0.76}\, T^{0.6}$. Such a behaviour of the diffusion coefficient would be in qualitative agreement if the scattering on impurities was the dominating scattering mechanism. This would require that all other scattering mechanisms could be

neglected in comparison with impurity scattering. We believe such an explanation to be unlikely. Firstly, rough quantitative estimates of the scattering rate on impurities indicate that this rate is much smaller than required to explain the data for τ_c. Secondly, the analysis of the data above 1 K strongly suggests that incoherent hopping of localized muons occurs in that temperature range. It is difficult to imagine that somewhat below 1 K the muons then abruptly propagate freely, scattering only on the impurities. Thirdly, the data on the electric field gradient (v) in $\underline{\text{Al}}\text{Mn}_{50\text{ppm}}$ at 40 mK show that the muon is localized at or near a single interstitial site. This is also in contradiction to the assumption of free coherent motion between the impurities, since the muon would be delocalized in that case.

Since a simple uniform diffusion cannot explain the data observed in the region below 1 K we have to consider more complicated models involving a change of the motional process during the muon lifetime.

The least complicated of these is again *trapping preceded by a diffusive motion*. At the very lowest temperatures the muons are assumed to stay in the traps for their remaining lifetime.

The fit of the data to the two-state model resulted in

$$\tau_1^{-1} \propto c^{0.76}\, T^{-0.6} \ .$$

This interpretation of the damping rate presupposed that strong motional narrowing prevails in the diffusive state.

The dependence below 1 K immediately excludes any phonon-induced process from reaching such low temperature traps. The low-temperature traps must therefore be reached by a coherent process. Since the conditions are somewhat different if the transport is capture-controlled or diffusion-controlled these two cases will now be discussed separately.

The capture-controlled process requires a coherence length $\ell \gg r_t$. As discussed above, such a situation is not likely to occur because of scattering processes due to electrons and remaining impurities. Still, if it were operative,

$\tau_1 = \sigma_{abs} v \times c$ should be independent of T for deep traps [see Eq. (20) and the subsequent text], which is not observed. More complicated temperature dependences than $\propto v^{-1}$ for σ_{abs} could occur for extended traps but are expected to be typical for each impurity whereas we observe an almost universal behaviour.

The most appealing of the "simple" trapping processes is therefore a *diffusion-controlled trapping preceded by a coherent motion of the type* $\ell < r_t$. In this case the capture rate is expected to be given by Eq. (19) with $D \propto v^2\tau$. With zJ_{eff} estimated to be of the order of 1 meV we expect $zJ_{eff} >> kT$ to hold below 1 K and the velocity of a thermalized muon should be proportional to $T^{\frac{1}{2}}$. We deduce from this interpretation the behaviour of the transport scattering rate which delimits coherent diffusion; explicitly

$$\tau^{-1} \propto c^{0.24}\, T^{1.6} \quad . \tag{3.2}$$

The dependences of this scattering rate have been listed in Table 1 for various possible processes. We note that our result for τ^{-1} is in obvious disagreement with the behaviour resulting from phonon scattering. In other words, the T^9 behaviour predicted by Kagan and Klinger[25], or a variant of it, is not observed. The behaviour of the transport scattering rate given above agrees roughly with that resulting from electron scattering. However, the residual dependence on concentration and the precise temperature power are not understood.

The fact that trapping occurs in O-sites instead of T-sites as at high temperature is a serious unsolved problem; it is probably connected with the different nature of the process by which the traps are reached (the low temperature trapping might occur further out from the impurity centres). It may be noted that the smaller depolarization for Li-doping as compared to that for Mn-doping of similar concentration (70 ppm) means a longer trapping time, i.e. a longer time of stay in the coherent regime for the case of Li-doping. Although the difference is not large, this fact indicates a smaller trapping radius for Li than for Mn, as expected.

All the observed facts i) to v) can therefore be said to fit qualitatively into a picture of coherent diffusion-limited motion before trapping. The precise power laws are still not reproduced, but the data provide sgrong evidence for the existence of coherent motion in this temperature range, for samples of sufficient purity.

One can also consider more complicated physical pictures, but we have not yet worked these out in detail. For instance, one can assume that the muons first perform rapid coherent motion and then enter into regions where they get localized but continue to diffuse by an incoherent process. The region where the transition between both types of motion occurs should be strongly disturbed (of the order of zJ_{eff}); however, only energies of the order of k_BT are available for thermal activation. Hence the incoherent process would most likely consist of a sequence of steps which lead more deeply into the trap. This would give a temperature-independent contribution to the depolarization, and the temperature variation deduced for coherent diffusion would be slightly increased.

The interpretation of our results below and above 1 K implies a transition from coherent to incoherent diffusion around this temperature. Comparing the experimental transition temperature of $\sim$ 1 K with the prediction of small polaron theory which is in the order of some tenths of the Debye temperature, again large discrepancies between experiment and theory become obvious. A possible way out of these difficulties might be the consideration of electron-scattering processes which are not related to the vibrational properties of the Al lattice. Our order of magnitude estimate of 0.1 K is certainly encouraging enough for further investigations.

Finally, some comments should be made on the possibility of capture from a metastable, non-self-trapped state, as suggested by Browne and Stoneham[11]. In this theory the muons perform diffusive motion in extended states with a mean free path limited by scattering on the impurities. The authors assume $\ell \propto c^{-1/3}$ in apparent contradiction with the accepted theory[64] of transport of, for example, electrons in band states. If transport is limited by scattering on impurities, ℓ should be proportional to c. Furthermore, they use the expression (19) for diffusion-limited trapping, whereas their assumption on the metastable state ($\ell > r_t$) means a capture-limited trapping. Although a motion in a metastable state before trapping at low temperature cannot be excluded, it is doubtful whether their theory can be modified so as to give a better description of the results for Al and Al alloys than the one presented here.

6. CONCLUSIONS

A number of questions concerning the nature of motion of light interstitials, especially for the case of positive muons, were raised in the Introduction and in the review of the theory of diffusion. Summing up the arguments of the previous Section we can draw the following conclusions from the present experiments:

i) The diffusion mechanisms of muons in Al appear to be different above and below 1 K. Above 1 K the muons perform incoherent hopping, whereas below 1 K they diffuse by coherent transfer (at least in parts of those of our samples that are sufficiently pure).

ii) Above 1 K, muons are trapped at substitutional impurities. The capture process is diffusion-limited trapping at single impurities.

iii) The linear temperature dependence found for the incoherent hopping rate is in contradiction with conventional small polaron theory; it is typical for a one-phonon process. However, the theories of one-phonon processes do not apply to the present case, with the exception of possible alternating transitions between O- and T-sites.

iv) The trapping regions around each impurity are extended, comprising many interstitial sites. The size of these regions is not directly correlated with the long-range strain field of the impurity used.

v) In pure Al the motional process is of such a nature that practically complete motional narrowing takes place down to 100 mK. Because of motional narrowing, the regime of coherent motion can only be studied indirectly in μSR experiments as a stage preceding trapping at low temperatures[65].

vi) The analysis of depolarization below 1 K in Al alloys suggest trapping controlled by coherent diffusion. The resulting diffusion coefficient is then proportional to $T^{-0.6}$. The temperature dependence is in disagreement with the predictions of conventional small-polaron theory, but it is in rough agreement with the predictions of scattering of conduction electrons on the muon.

vii) The transition temperature of approximately 1 K between the region of incoherent hopping and the region of coherent transfer is lower than that predicted by small-polaron theory.

viii) The O-sites are the lowest energy sites for muons at the lowest temperatures. At intermediate temperatures the muons seem to move over T-sites as well as O-sites. At the Mn-trapping peak in Al the T-site is the most stable one, probably lowered in energy by the closeness of an Mn atom at a substitutional site.

In our opinion the essential results of the present investigation are: firstly, clear evidence for both incoherent hopping and coherent motion of muons in pure Al; and, secondly, the fact that the results are not adequately described by the current small-polaron theory of the motion of light interstitials in metals, which predicts strong temperature dependences of incoherent hopping (T^7) and coherent diffusion (T^{-9}), while our results indicate weak temperature dependences (T and $T^{-0.6}$, respectively). Also the transition temperature of about 1 K between dominating coherent diffusion and dominating incoherent hopping has not been predicted by theory.

Both the weak temperature dependences as well as the low transition temperature indicate that electron scattering might play an important role at low temperature.

Since Al so far is the only metal which has been studied systematically at low temperature, it is of great importance to extend the investigations to other materials in order to find out whether the observed transport phenonena are of a universal nature.

Acknowledgements

We are indebted to G. Jangerberg for technical assistance in preparing the samples and to H. Beske and M.W. Brunner for analytical support. The help of J. Chappert and A. Kuijk in some of the experiments is gratefully acknowledged.

REFERENCES AND FOOTNOTES

1) I.I. Gurevich, E.A. Meleshko, I.A. Muratova, B.A. Nikolsky, V.S. Roganov, V.I. Selivanov and B.V. Sokolov, Phys. Lett. 40A, 143 (1972).

2) Proc. First Int. Topical Meeting on Muon Spin Rotation, Rorschach, 4-7 September 1978, edited by F.N. Gygax, W. Kündig and P.F. Meier, Hyperfine Interactions 6 (1979).

3) Proc. Second Int. Topical Meeting on Muon Spin Rotation, Vancouver, 11-15 August 1980, edited by J.H. Brewer and P.W. Percival, Hyperfine Interactions 8 (1981).

4) O. Hartmann, E. Karlsson, P. Pernestål, M. Borghini, T.O. Niinikoski and L.O. Norlin, Phys. Lett. 61A, 141 (1977).

5) O. Hartmann, E. Karlsson, L.O. Norlin, D. Richter and T.O. Niinikoski, Phys. Rev. Lett. 41, 1055 (1978).

6) W.J. Kossler, A.T. Fiory, W.F. Lankford, K.G. Lynn, R.P. Minnich and C.E. Stronach, Hyperfine Interactions 6, 295 (1979).

7) O. Hartmann, E. Karlsson, L.O. Norlin, T.O. Niinikoski, K.W. Kehr, D. Richter, J.M. Welter, A. Yaouanc and J. LeHéricy, Phys. Rev. Lett. 44, 337 (1980).

8) J.H. Brewer, K.M. Crowe, F.N. Gygax and A. Schenck, in *Muon Physics, Vol. III, Chemistry and Solids*, edited by V.W. Hughes and C.S. Wu (Academic, New York, 1975), p. 3.

9) D. Emin, Adv. Phys. 22, 57 (1973).

10) D. Emin and T. Holstein, Phys. Rev. Lett. 36, 323 (1976).

11) A.M. Browne and A.M. Stoneham, AERE preprint TP. 880 (1980).

12) M. Manninen and R.M. Nieminen, J. Phys. F 9, 1333 (1979).

13) L.M. Kahn, F. Perrot and M. Rasolt, Phys. Rev. B 21, 5594 (1980).

14) F. Perrot and M. Rasolt, Phys. Rev. B 23, 6534 (1981).

15) C. Berthier and M. Menier, J. Phys. F 7, 515 (1977).

16) J.P. Bugeat, A.C. Chami and E. Ligeon, Phys. Lett. 58A, 127 (1976).

17) J.P. Bugeat and E. Ligeon, Phys. Lett. 71A, 93 (1979).

18) A.M. Stoneham, J. Phys. F 2, 417 (1972).

19) P.W. Anderson, Phys. Rev. 109, 1492 (1958).

20) See, for example, D. Thouless, in *Ill Condensed Matter*, Les Houches Session, 3 July-18 August 1978, edited by R. Balian, R. Maynard and G. Toulouse (North Holland, Amsterdam, 1979), p. 1.

21) G. Leibfried and N. Breuer, *Point Defects in Metals I*, in Springer Tracts on Modern Physics, edited by G. Höhler, (Springer, Berlin, 1978), Vol. 81, p. 163.

22) B. Baranowski, S. Majchrzak and T.B. Flanagan, J. Phys. C 7, 2791 (1974).

23) W.B. Pearson, *Lattice Spacings and Structure of Metals and Alloys* (Pergamon, Oxford, 1958), p. 346.

24) T. Holstein, Ann. Phys. (NY) 8, 325, 343 (1959).

25) Yu. Kagan and M.J. Klinger, J. Phys. C 7, 2791 (1974).

26) K.W. Kehr, Proc. Second JIM Int. Symposium Hydrogen on Metals, Minakami, 26-29 Nov., 1979, Suppl. Trans. Jpn. Inst. Met. 21, 181 (1980).

27) A.F. Andreev and I.M. Lifshitz, Sov. Phys.-JETP 29, 1107 (1969).

28) A.F. Ioffe and A.R. Regel, Prog. Semicond. 4, 237 (1960).

29) C.P. Flynn and A.M. Stoneham, Phys. Rev. B1, 3966 (1970).

30) S. Fujii, J. Phys. Soc. Jpn. 46, 1833 (1979).

31) H. Teichler, Phys. Lett. 64A, 78 (1977).

32) M. Camani, F.N. Gygax, W. Rüegg, A. Schenck and H. Schilling, Phys. Rev. Lett. 39, 836 (1977).

33) D. Herlach, in *Recent Developments in Condensed Matter Physics*, Vol. 1 (ed. J.T. Devreese) Plenum Press, N.Y. 1981.

34) D. Herlach et al., unpublished.

35) J.A. Sussmann, Phys. Kondens. Materie 2, 146 (1964).

36) H. Teichler and A. Seeger, Phys. Lett. 82A, 91 (1981).

37) H. Teichler, Hyperfine Interactions 8, 505 (1981).

38) K.G. Petzinger, unpublished.

39) M. Borghini, T.O. Niinikoski, J.C. Soulié, O. Hartmann, E. Karlsson, L.O. Norlin, K. Pernestål, K.W. Kehr, D. Richter and E. Walker, Phys. Rev. Lett. 40, 1723 (1978).

40) E. Karlsson, Hyperfine Interactions 8, 647 (1981).

41) D. Richter, in *Nuclear and Electron Resonance Spectroscopies applied to Materials Science*, Proc. Mat. Res. Soc. Ann. Meeting, Boston, Mass., 1980, edited by E.N. Kaufmann and G.K. Shenoy (North Holland, New York, 1981), p. 233.

42) One could imagine traps which consist of high barriers, and where the ground state level is not lowered compared to the host. The capture of a muon on such a trap would be extremely unlikely.

43) T.R. Waite, Phys. Rev. 107, 463 (1957).

44) K. Schröder and K. Dettmann, Z. Phys. B 22, 343 (1975).

45) C.H. Hodges, J. Phys. F 4., L 230 (1974).

46) I.K. Mackenzie, T.L. Koo, A.B. McDonald and B.T.A. McKee, Phys. Rev. Lett. 19, 946 (1967).

47) R. Lenzi, P. Podini, R. Reverberi and K. Pernestål, Nucl. Instrum. Methods 150, 575 (1978).

48) K.W. Kehr, D. Richter, J.M. Welter, O. Hartmann, L.O. Norlin, E. Karlsson, T.O. Niinikoski, J. Chappert and A. Yaouanc, Hyperfine Interactions 8, 681 (1981).

49) W.J. Kossler, A.T. Fiory, W.F. Lankford, L. Lindemuth, K.G. Lynn, S. Majahan, R.P. Minnich, K.G. Petzinger and C.E. Stronach, Phys. Rev. Lett. 41, 1558 (1978).

50) A. Schenck, *On the application of polarized positive muons in solid state physics*, in *Nuclear and Particle Physics at Intermediate Energies*, edited by J.B. Warren (Plenum, New York, 1976), p. 159.

51) K.W. Kehr, G. Honig and D. Richter, Z. Phys. B 32, 49 (1978).

52) K.W. Kehr, D. Richter and G. Honig, Hyperfine Interactions 6, 219 (1979).

53) K.G. Petzinger, R.L. Munjal and E. Zaremba, Hyperfine Interactions 6, 223 (1979).

54) R. Kubo, in *Fluctuation, Relaxation, and Resonance in Magnetic Systems*, edited by D. Ter Haar (Oliver and Boyd, Edinburg, 1962), p. 23.

55) R. Kubo, J. Phys. Soc. Jpn. 9, 935 (1954).

56) O. Hartmann, unpublished.

57) T. McMullen and E. Zaremba, Phys. Rev. B18, 3026 (1978).

58) S. Fujii and Y. Uemura, Solid State Commun. 26, 761 (1978).

59) S. Fujii, J. Phys. Soc. Jpn. 46, 1843 (1979).

60) J.A. Van Vleck, Phys. Rev. 74, 1168 (1948).

61) O. Hartmann, Phys. Rev. Lett. 39, 832 (1977).

62) D. Richter and T. Springer, Phys. Rev. B 18, 126 (1978).

63) K. Werner, private communication.

64) J.M. Ziman, *Electrons and Phonons* (University Press, Oxford, 1960).

65) A. Yaouanc, to be published in Physics Letters.

Table 1

Temperature dependence of scattering rates and diffusion coefficients for small-polaron motion

a) *Coherent diffusion*

Scattering process	Scattering rate τ^{-1}	Diffusion coefficient	
		$zJ_{eff} \ll k_B T$	$zJ_{eff} \gg k_B T$
Phonon scattering on interstitial	T^9	T^{-9}	T^{-8}
Phonon scattering on fluctuating tunnelling transfer	T^7	T^{-7}	T^{-6}
Electron scattering	T	T^{-1}	T^0
Scattering on impurities	cT^0	T^0/c	T/c

b) *Incoherent diffusion*

Interaction process	Diffusion coefficient
One-phonon process (requires energy difference ΔE)	$(\Delta E)^2 T$
Two-phonon process	T^7 (T^3)
Multiphonon process	$T^{\frac{1}{2}} \exp(-E_a/k_B T)$

Table 2

Determination of the concentration of the alloying elements in Al by atomic absorption spectroscopy

Alloy designation	Nominal concentration (at. ppm)	Measured concentration (at. ppm)	Number of sample uptakes	Number of determinations
AlAg	117	116.8 ± 3.8	2	6
AlLi	75	75.8 ± 4.0	2	10
AlMn	42	41.5 ± 4.0	1	3
AlMn	5	4.6 ± 0.8	1	7
AlMn	10	9.9 ± 0.1	1	6
AlMn	42	41.8 ± 5.6	1	10
AlMn	57	57.6 ± 2.0	3	20
AlMn	70	69.9 ± 1.6	2	6
AlMn	1300	1137.0 ± 53.0	3	12
AlMn	1300	1296.0 ± 87.0	2	15

Table 3

Determination of impurities in high purity Al and different Al alloys by spark-source mass spectrometry. The concentrations are given in at. ppm.

	Pure Al	AlAg	AlLi	AlMg	AlMn
Li	< 0.02	< 0.3		< 0.08	< 0.08
Be	< 0.02	< 0.06	< 0.6	< 0.06	< 0.06
B	0.006	< 0.1	< 0.5	< 0.4	< 0.5
C	6.0	< 0.2	3.1 ± 1.9	1.2 ± 0.9	5.8 ± 1.8
N	0.32	0.8 ± 0.5	0.7 ± 0.2	0.1 ± 0.02	0.2 ± 0.02
F	0.024	< 0.3	< 0.4	< 0.7	< 0.6
Ne		< 0.3	< 0.1	< 0.3	< 0.3
Na	0.015	0.2 ± 0.04	1.0 ± 0.3	< 0.5	0.1 ± 0.04
Mg	(1.5)	1.0 ± 0.04	0.9 ± 0.2	521 ± 270*	< 2
Si	< 0.1	< 0.7	< 0.3	< 1	< 1
P	< 0.1	< 0.5	< 0.2	< 0.4	0.02 ± 0.1
S	0.89	< 0.5	< 0.9	< 0.4	0.05 ± 0.2
Cl	< 0.1	< 0.3	< 0.6	< 0.2	< 0.2
Ar		< 0.1	< 0.1	< 0.1	< 0.2
K	0.83	< 0.5	< 0.3	< 0.1	< 0.6
Ca	0.27	< 0.2	< 0.3	0.1 ± 0.01	< 0.5
Sc	< 0.02	< 0.1	< 0.6	< 0.5	< 0.3
Ti	< 0.3	< 0.3	< 0.6		< 0.3
V	< 0.15	< 0.3	0.5 ± 0.02		< 0.2
Cr	< 0.06	< 0.5	< 0.5		1.1 ± 0.4
Mn	< 0.025	< 0.2	< 0.5		115 ± 19
Fe	0.2	0.3 ± 0.08	0.2 ± 0.02		4.0 ± 1.6
Co	< 0.1	< 0.4	< 0.3		< 0.1
Ni	< 0.15	< 0.2	< 0.3		< 0.5
Cu	< 0.025	0.2 ± 0.07	0.4 ± 0.1		0.2 ± 0.08
Zn	< 0.11	< 0.1	0.6 ± 0.2		< 0.5
Ga	1.8	< 0.5	< 0.5		
Ag	< 0.3	94 ± 33			

Table 4

Fitting parameters of the two-state model
for the different Al samples

Sample	Conc. (at. ppm)	Γ_1^{-1} ($\times 10^4$ s^{-1})	α	Γ_0^{-1} ($\times 10^6$ s^{-1})	E_a (K)
AlMn	42	1.62 ± 0.12			
AlMn	57	2.02 ± 0.14	0.89 ± 0.03	28.6 ± 3.5	120 ± 6
AlMn	70	2.43 ± 0.14			
AlLi	75	4.0 ± 1.0	0.36 ± 0.07	0.85 ± 0.15	145 ± 27
AlMg	42	3.3 ± 0.4	0.54 ± 0.04	2.03 ± 0.44	142 ± 7
AlAg	117	3.9 ± 0.4	0.45 ± 0.05	2.45 ± 0.32	87 ± 7

Table 5

Lattice expansion of Al due to substitutional impurities,
deduced from Pearson[24)]

Impurity	Mn	Mg	Li	Ag
$\Delta a/a$ for 1 at. %	-1.5×10^{-3}	0.99×10^{-3}	-1.1×10^{-4}	$< 10^{-5}$
ΔV ($\mathring{A}^3$)	-7.42	4.9	-0.54	< 0.05

Figure captions

Fig. 1 : Gaussian damping parameter σ for Al and AlMn polycrystalline samples. The external field is B_0 = 520 G for $AlMn_{42ppm}$, 150 G for the others.

Fig. 2 : Gaussian damping parameter σ for AlMn single crystal samples. The 1300 ppm sample was measured in a 220-250 G field, the others in a 130-150 G field. At these field values there should only be small differences between the different orientations (see Fig. 7).

Fig. 3 : The trapping-peak region around 15 K for AlMn samples of various concentrations. Some of the samples have been measured at more than one magnetic field, which is indicated by different symbols. The 42 ppm points are at higher field than the others except for the three points marked with a double ring. These were measured at 130 G and scaled down 15% in order to accommodate for the field dependence of the line width.

Fig. 4 : Gaussian damping parameter σ for Al with various doping elements for T = 2-100 K; B_0 = 150 G.

Fig. 5 : Gaussian damping parameter σ for AlMn, AlLi, and AlAg samples below 2 K (at B_0 = 150 G).

Fig. 6 : Inverse correlation times τ_c^{-1} for various AlMn samples as a function of temperature. The τ_c values were evaluated from Eq. (24). The field lines are individual fits to a T^{ν} dependence with the parameter ν given in the figure. A global fit of the data gives ν = 0.60 (4).

Fig. 7 : Magnetic field dependence of the damping parameter σ for various AlMn samples and temperatures. The 0.04 K data show an octahedral interstitial site symmetry, while the two measurements from 15 K show a tetrahedral site symmetry.

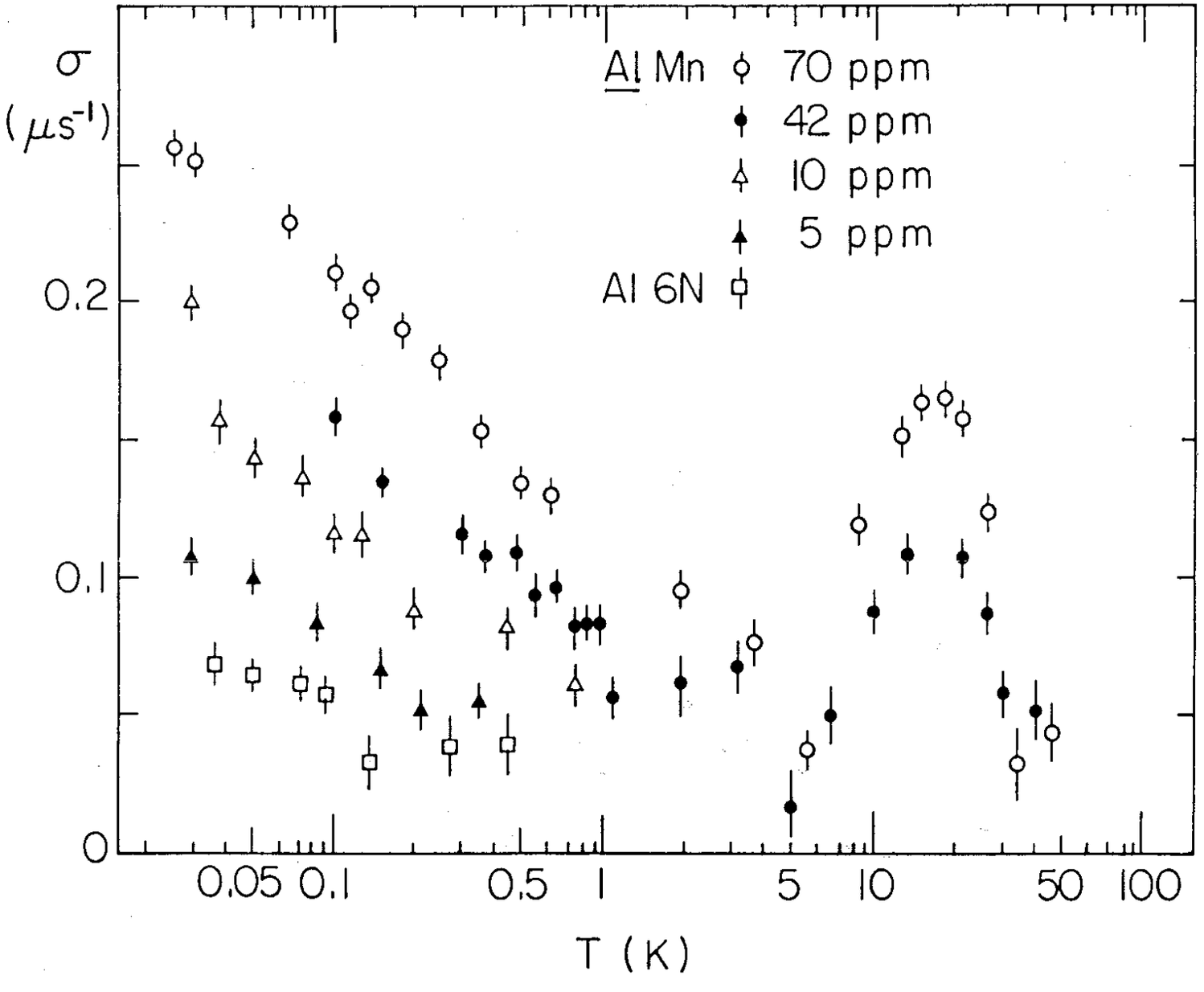
σ
(μs⁻¹)
Al Mn 70 ppm
42 ppm
10 ppm
5 ppm
Al 6N
0.2
0.1
0
0.05
0.1
0.5
1
5
10
50
100
T (K)

Fig. 1

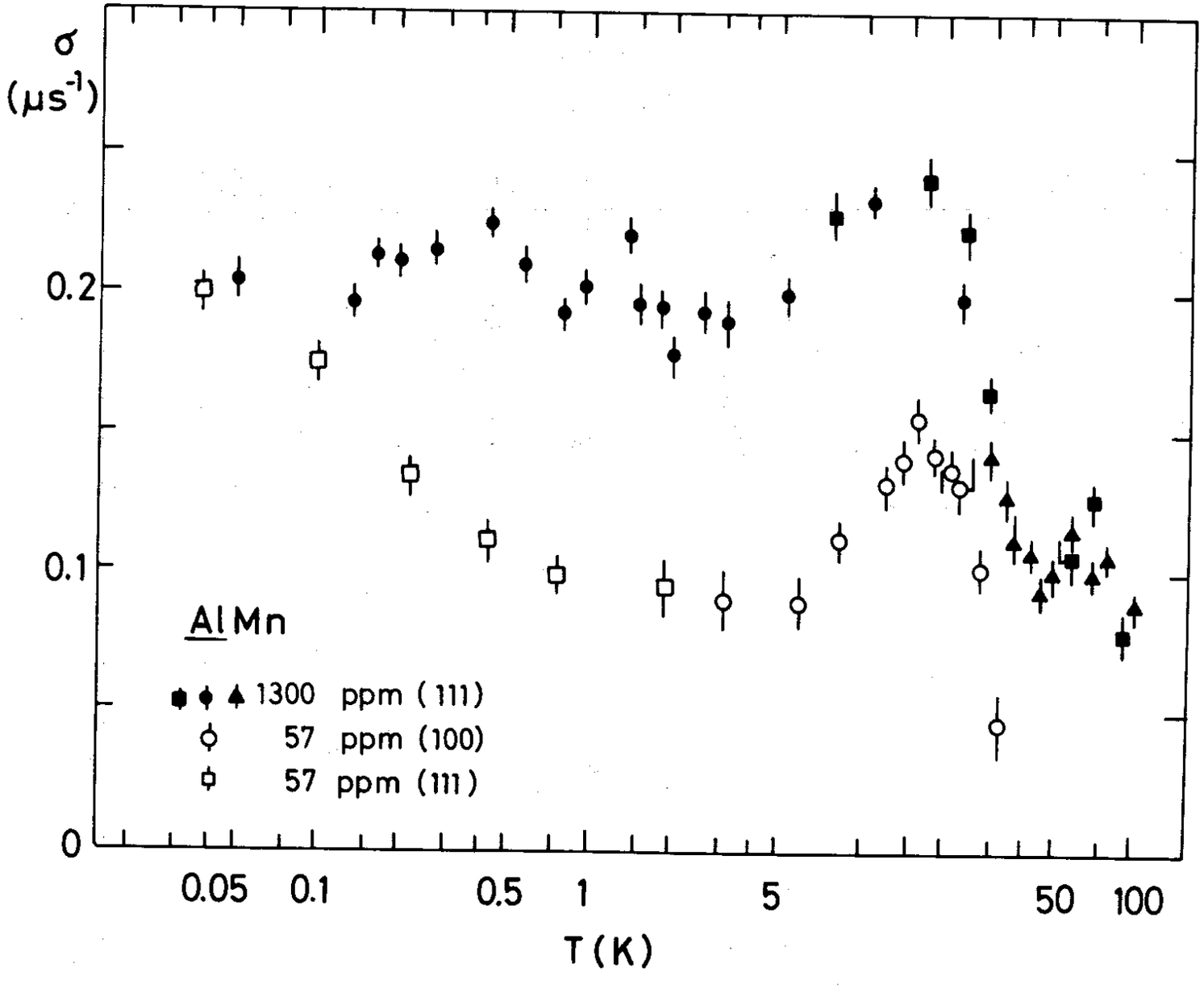
σ
(μs⁻¹)
0.2
0.1
0
AlMn
1300 ppm (111)
57 ppm (100)
57 ppm (111)
0.05
0.1
0.5
1
5
50
100
T(K)

Fig. 2

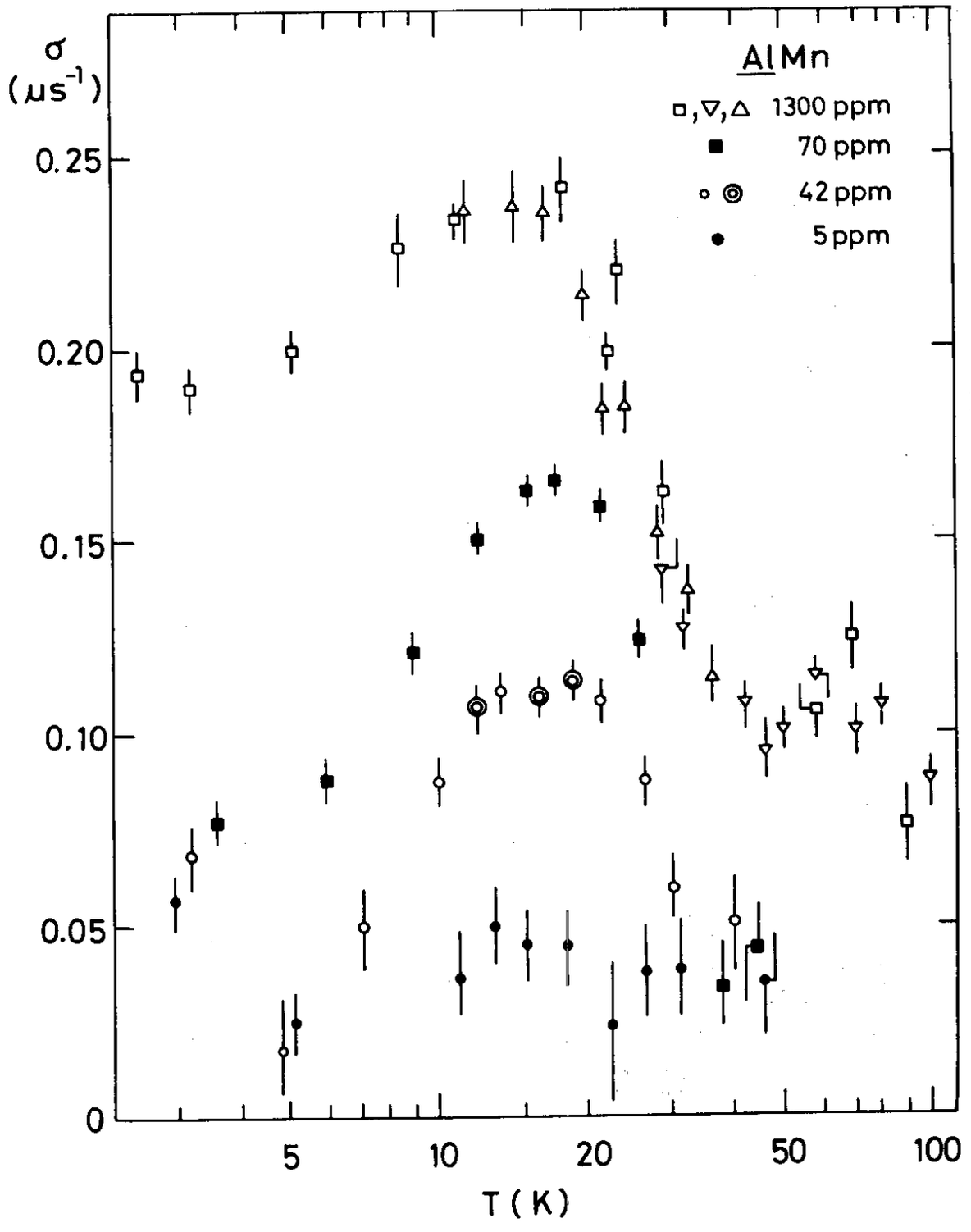
σ
(μs⁻¹)
AlMn
□,▽,△ 1300 ppm
■ 70 ppm
○ ◎ 42 ppm
● 5 ppm
0.25
0.20
0.15
0.10
0.05
0
5
10
20
50
100
T (K)

Fig. 3

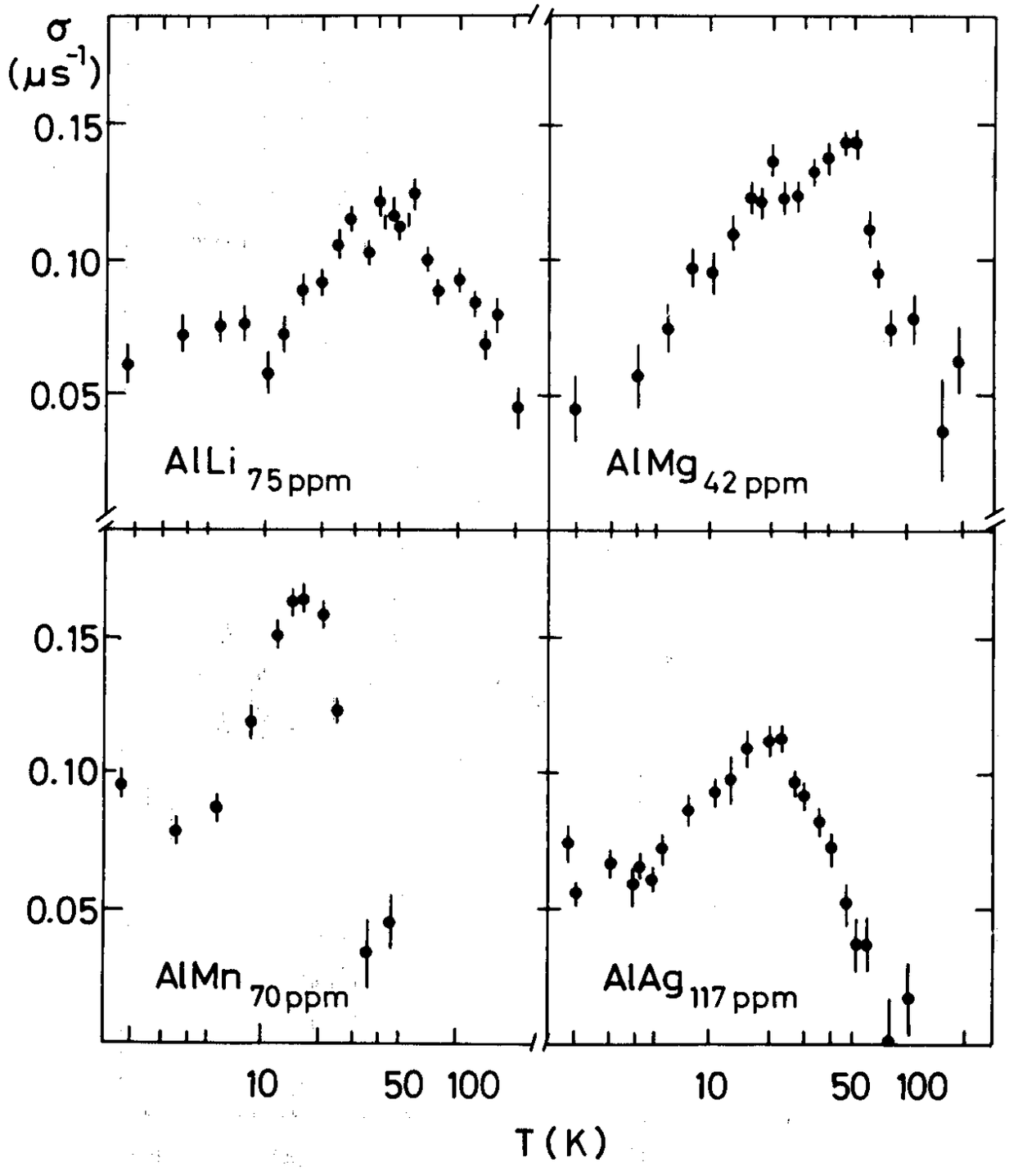
σ
(μs⁻¹)
0.15
0.10
0.05
AlLi 75 ppm
AlMg 42 ppm
AlMn 70 ppm
AlAg 117 ppm
10
50
100
T (K)

Fig. 4

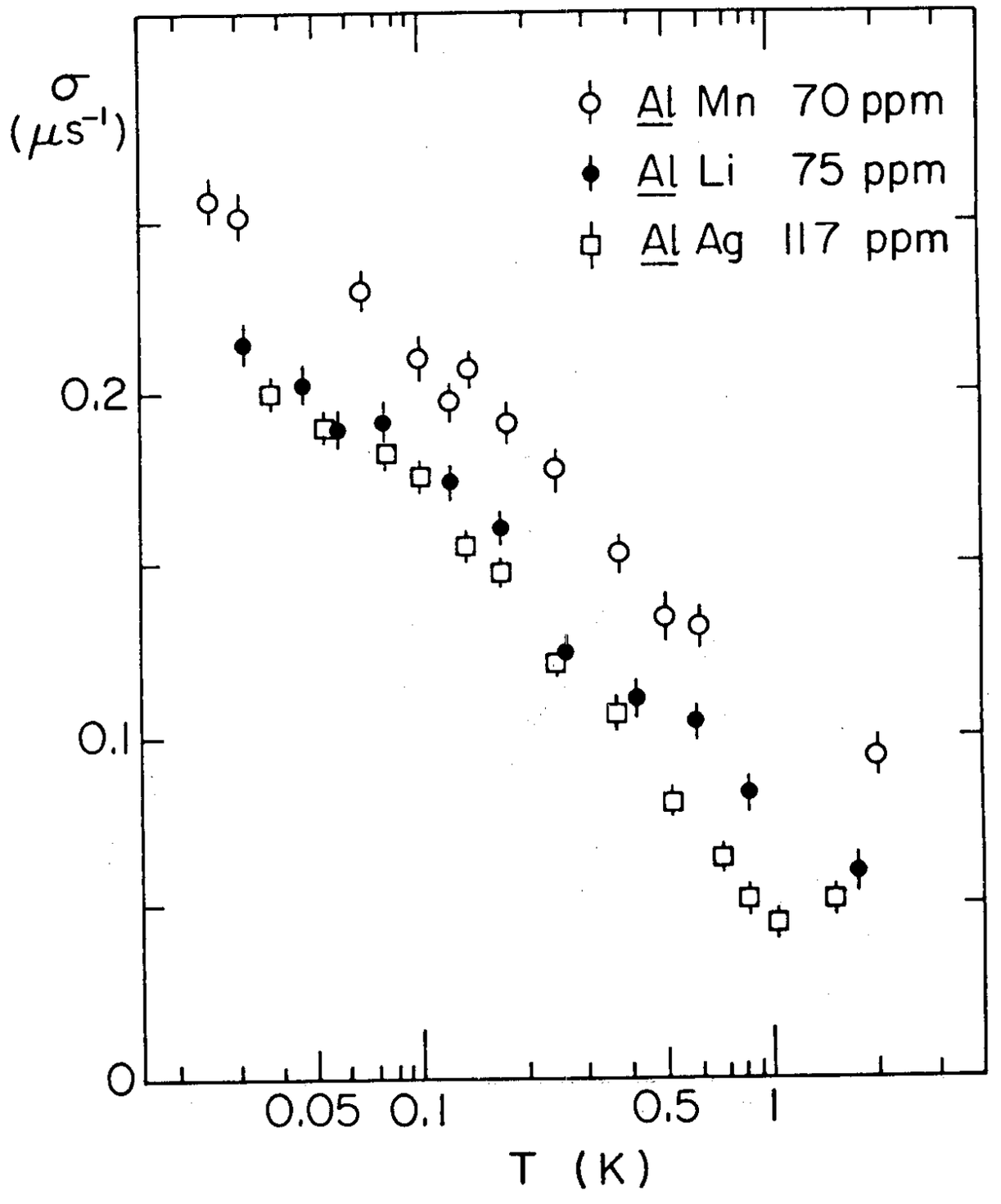

Fig. 5

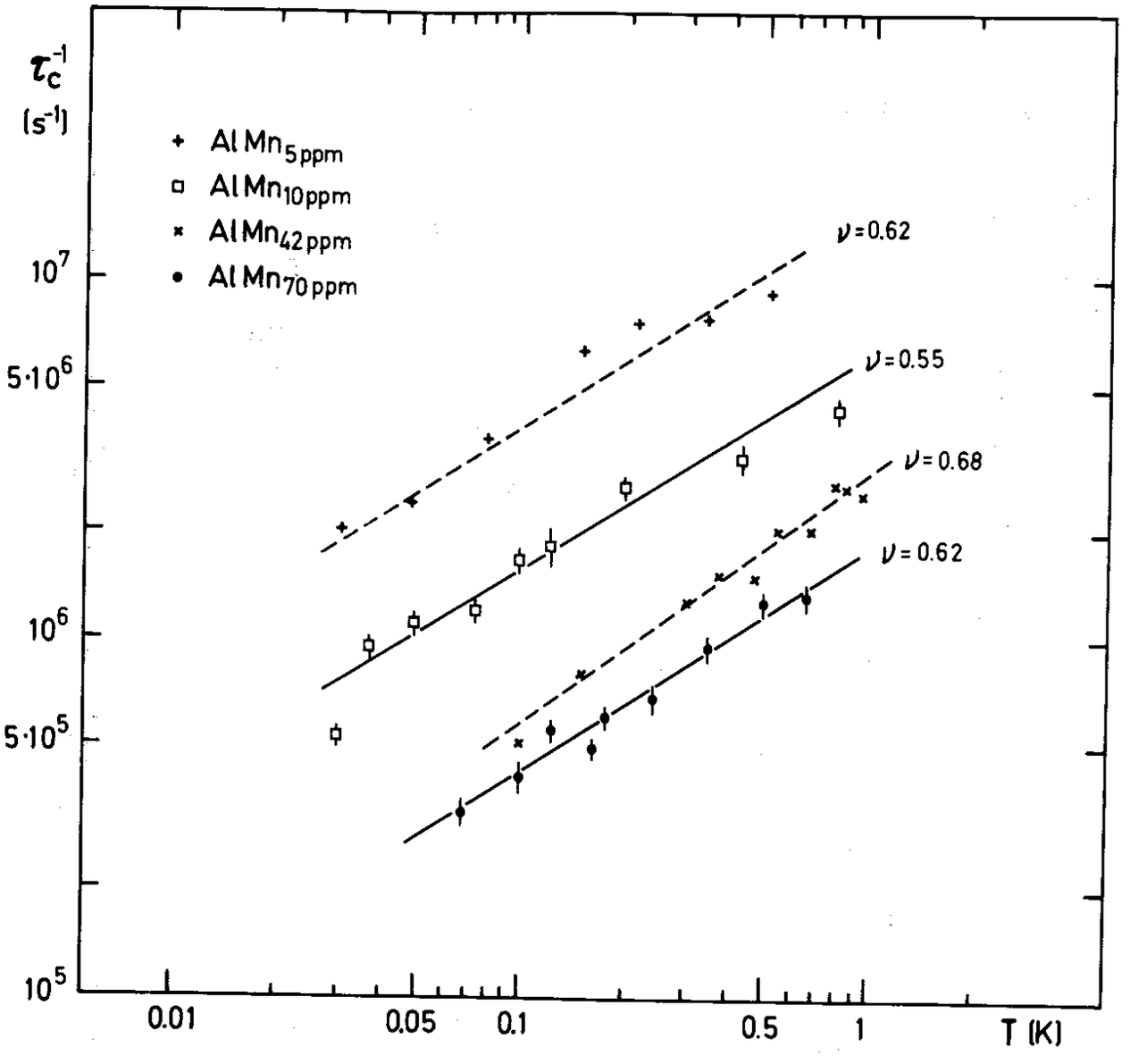
τ_c^{-1} (s^{-1})
Al Mn 5 ppm
Al Mn 10 ppm
Al Mn 42 ppm
Al Mn 70 ppm
$\nu = 0.62$
$\nu = 0.55$
$\nu = 0.68$
$\nu = 0.62$
10^7
$5 \cdot 10^6$
10^6
$5 \cdot 10^5$
10^5
0.01
0.05
0.1
0.5
1
T (K)

Fig. 6

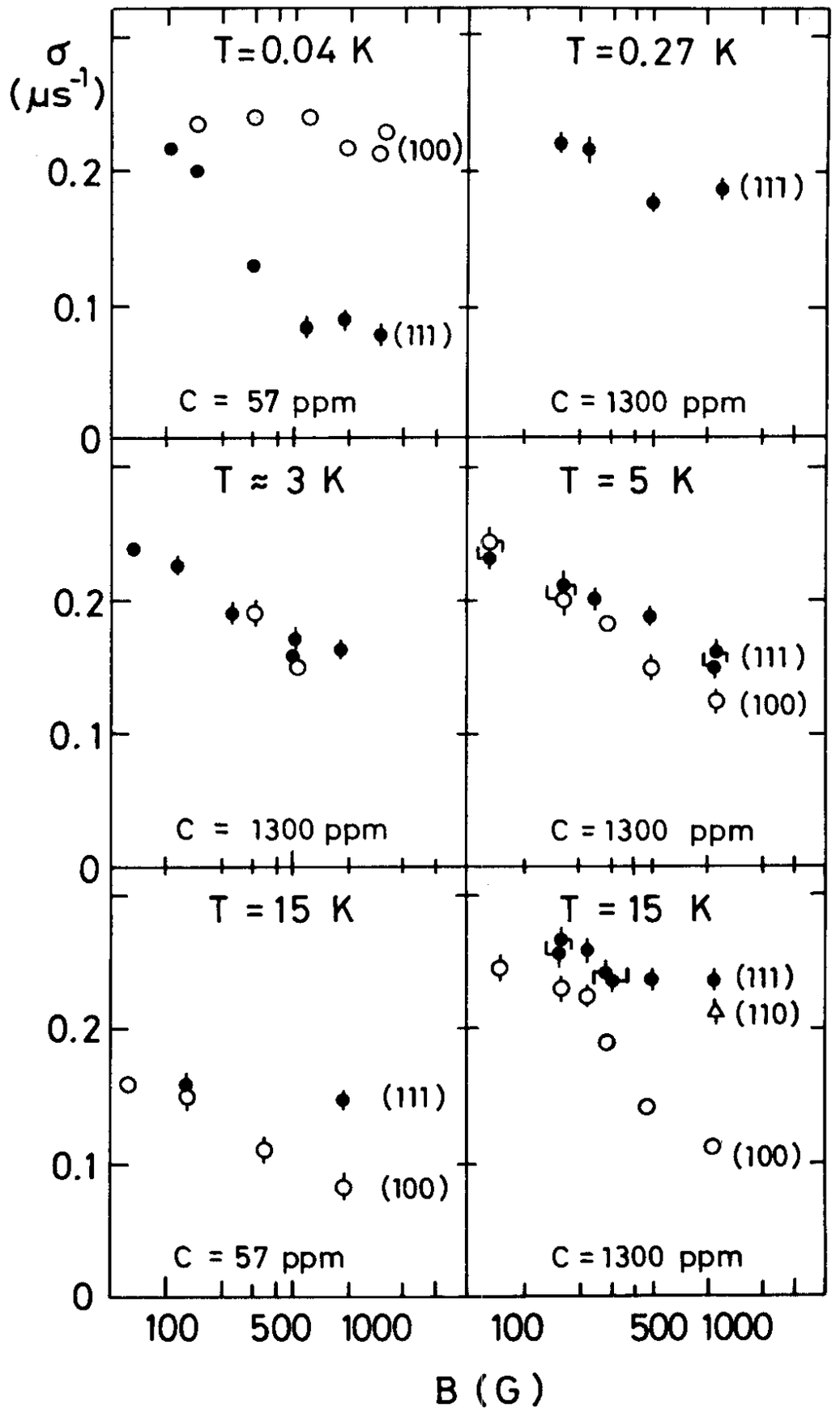
σ (μs⁻¹)
T=0.04 K
T=0.27 K
T ≈ 3 K
T = 5 K
T = 15 K
T = 15 K
(100)
(111)
(110)
C = 57 ppm
C = 1300 ppm
0
0.1
0.2
100
500
1000
B (G)

Fig. 7